Theor. Comput. Fluid Dyn. (2008) 22: 157–187
DOI 10.1007/s00162-007-0067-9

ORIGINAL ARTICLE

M. Breuer · B. Jaffrézic · K. Arora

Hybrid LES–RANS technique based on a one-equation near-wall model

Received: 3 May 2006 / Accepted: 4 September 2007 / Published online: 26 October 2007

Abstract In order to reduce the high computational effort of wall-resolved large-eddy simulations (LES), the present paper suggests a hybrid LES–RANS approach which splits up the simulation into a near-wall RANS part and an outer LES part. Generally, RANS is adequate for attached boundary layers requiring reasonable CPU-time and memory, where LES can also be applied but demands extremely large resources. Contrarily, RANS often fails in flows with massive separation or large-scale vortical structures. Here, LES is without a doubt the best choice. The basic concept of hybrid methods is to combine the advantages of both approaches yielding a prediction method, which, on the one hand, assures reliable results for complex turbulent flows, including large-scale flow phenomena and massive separation, but, on the other hand, consumes much fewer resources than LES, especially for high Reynolds number flows encountered in technical applications. In the present study, a non-zonal hybrid technique is considered (according to the signification retained by the authors concerning the terms zonal and non-zonal), which leads to an approach where the suitable simulation technique is chosen more or less automatically. For this purpose the hybrid approach proposed relies on a unique modeling concept. In the LES mode a subgrid-scale model based on a one-equation model for the subgrid-scale turbulent kinetic energy is applied, where the length scale is defined by the filter width. For the viscosity-affected near-wall RANS mode the one-equation model proposed by Rodi et al. (J Fluids Eng 115:196–205, 1993) is used, which is based on the wall-normal velocity fluctuations as the velocity scale and algebraic relations for the length scales. Although the idea of combined LES–RANS methods is not new, a variety of open questions still has to be answered. This includes, in particular, the demand for appropriate coupling techniques between LES and RANS, adaptive control mechanisms, and proper subgrid-scale and RANS models. Here, in addition to the study on the behavior of the suggested hybrid LES–RANS approach, special emphasis is put on the investigation of suitable interface criteria and the adjustment of the RANS model. To investigate these issues, two different test cases are considered. Besides the standard plane channel flow test case, the flow over a periodic arrangement of hills is studied in detail. This test case includes a pressure-induced flow separation and subsequent reattachment. In comparison with a wall-resolved LES prediction encouraging results are achieved.

Keywords Hybrid LES–RANS · Interface and interface criteria · Modeled and resolved scales · DES

PACS 47.27.E–, 47.27.N–, 02.60.–x

Communicated by R.D. Moser.

M. Breuer (✉) · B. Jaffrézic · K. Arora
Institute of Fluid Mechanics, University of Erlangen–Nürnberg, Cauerstr. 4, 91058 Erlangen, Germany
E-mail: breuer@lstm.uni-erlangen.de

1 Introduction

It is well known that the prediction of complex separated unsteady flows based on the Reynolds-averaged Navier–Stokes (RANS) equations often does not yield satisfactory results. Unfortunately, even the use of the most modern turbulence models could not essentially improve the situation. Therefore, during the last decade, many researchers have paid more attention towards large-eddy simulation (LES) and direct numerical simulation (DNS) as alternative prediction methods. However, these alternatives are actually too expensive with respect to the required computer performance; this thesis is clear for DNS, but the situation with LES, if the development of supercomputers is taken into account, seems to be not so drastic. Nevertheless, the analysis carried out by Spalart et al. [42] shows that for Reynolds numbers of about 10^7, i.e., normal *aerodynamic* values, a computational grid consisting of a minimum of 10^{11} cells and a minimum of 5×10^6 time steps has to be used. Such huge computations are out of reach for the next couple of decades. Consequently, LES is a highly promising technique for the prediction of complex turbulent flows including large-scale flow phenomena such as massive separation, large recirculation regions and vortex shedding [6], but it still suffers from the matter of fact that most turbulent flows of practical relevance cannot be computed. In order to go beyond the present state-of-the-art, extremely fine grids especially required for the resolution of the near-wall region (e.g., thin boundary layers) have to be avoided.

This circumstance was the main reason for developing new kinds of *hybrid* methods, which combine the main features of both LES and RANS simulations (see, e.g., [16,42–50,52,53]). The basic idea of all approaches is to restrict the application of the time-consuming LES prediction to regions which can hardly be predicted reasonably by RANS, but to rely on the "cheaper" RANS technique, wherever it is possible.

In spite of the widespread application of RANS predictions for turbulent flows, the main disadvantage of the method is clear: RANS describes flows in a statistical sense typically leading to time-averaged pressure and velocity fields. Generally, this approach is not able to distinguish between quasi-periodic large-scale and turbulent chaotic small-scale features of the flow field. This leads to huge problems when the flow field is governed by both phenomena. A typical representative is a bluff body flow. The RANS approach is not able to reproduce the unsteady characteristics of the flow field reasonably, resulting in an inadequate description of unsteady phenomena such as vortex formation and shedding. Partially, the situation might be improved by applying the unsteady Reynolds-averaged Navier–Stokes (URANS) equations combined with statistical models, sometimes also denoted as VLES (very large-eddy simulation) [45]. However, this concept is based on the assumption that a clear scale separation can be carried out between the largest-scale motion (e.g., vortex shedding) and all turbulence-induced small scales what is often not the case.

Thus, even with the help of sophisticated turbulence models, such as Reynolds stress models, which are usually semi-empirically closed containing about 6–9 empirical constants, it is often not possible to model large-scale phenomena adequately. LES, on the other hand, operates fully with unsteady fields of (filtered) physical values; the governing equations are the Navier–Stokes equations but, unlike the RANS approach, spatial filtering is applied instead of averaging in time, and turbulent stresses are divided into resolved and modeled components. In contradiction to *classical* turbulence models the small-scale motion can be described by extremely simple subgrid-scale models, often based on an algebraic eddy-viscosity concept, such as Smagorinsky's model [40]. As mentioned above, the main disadvantage of LES is the high computational costs resulting from extremely fine grids used for the direct prediction of the *non-modeled* vortical structures. A very fine resolution defined by $\Delta y^+_{1\text{st point}} = O(1)$, $\Delta x^+ = O(50)$, and $\Delta z^+ = O(15)$ is commonly required in the vicinity of solid walls for wall-resolved LES, where y, x and z denote the wall-normal, streamwise and spanwise direction, respectively. Additionally, very fine time steps have to be applied for resolving the turbulent scales in time.

For an hybrid method it is natural that RANS is applied in those regions, where statistical turbulence models in general perform properly. Moreover, LES is used in regions, where large unsteady vortical structures are present, which should be resolved directly. Overall this strongly reduces the resolution requirements. For example, if RANS is applied for the prediction of attached boundary layers, this kind of division of the flow field then allows one to decrease the near-wall resolution in streamwise and spanwise direction dramatically since with the exception of the wall-normal direction the resolution does not have to be very high for RANS [27]. These facts raise the hope that hybrid LES–RANS techniques can be used with acceptable effort even for high Reynolds numbers, typically encountered in technical applications.

Several hybrid LES–RANS strategies were suggested during the last few years. Nevertheless, the most widely known is the detached-eddy Simulation (DES) [27] based on a slight modification of the one-equation Spalart–Allmaras (SA) RANS model [41]. The target aimed by the DES designers was external aerodynamic

flows at high Re. Therefore, the main application area should be unsteady turbulent flows with large separation regions for which RANS predictions do not work properly. DES modeling of non-separated flow typically leads to some problems as demonstrated by Nikitin et al. [27]. On the other hand, all DES applications of separated flows were mainly successful (see, e.g., [39,52]). Hence hybrid LES–RANS applications to such turbulent flows seem to be reasonable and reliable whose dynamics are defined by large-scale separated vortices playing a dominant role in the energy balance. Therefore, very often DES results for flows around complex geometries, e.g., the flow around an airplane carriage [47] and a forebody cross-section [48], are presented in the literature.

A variety of different hybrid concepts were proposed during the last years. A crude distinction between various proposals is given by *zonal* and *non-zonal* techniques. Nevertheless, these epithets tend to be differently interpreted, which can lead to a certain confusion. In order to avoid this situation, the definition retained by the authors is explained. By definition an hybrid LES–RANS method is the application of these two techniques within the same simulation selected according to their advantages. This leads to two distinct areas, namely the RANS and LES zones. In this sense, an hybrid LES–RANS technique is *zonal*. However, the various definitions of *zonal/non-zonal* are more precise and deal with the types of models selected in each mode (LES or RANS) or the manner of defining both zones, etc. Here, the authors are inclined to define these terms as the method used to select the LES and RANS modes. In the first case (*zonal* approach), the user predefines the LES and RANS regions prior to the start of the simulation through the grid design, an explicit border (e.g., y^+ value, wall distance, etc.) or the selection of domains not especially related to wall regions. Conversely, the *non-zonal* approach chooses (more or less) automatically the simulation technique within the computation and thus avoids the region predefinition. Here a gradual transition between both methods takes place which weakens the problem of setting up an appropriate coupling strategy between RANS and LES zones not available today. Furthermore, the term *seamless* has been proposed by Hanjalić et al. [17], but not detailed here, to specify that the "same model is applied throughout the flow with a continuous sub(-grid)-scale model modification".

Different examples of zonal/non-zonal approaches can be found, starting from the DES, which is defined as a non-zonal approach by the authors [39]. Nevertheless, by scrutinizing the switching criterion, which is based on the comparison of the RANS and LES length scales, a grid dependency is noticed. Thus the interface location is predefined by the grid design. Hence, depending on the definition chosen DES can be seen either as a zonal or a non-zonal method. The hybrid strategy outlined by Batten et al. [2] and named LNS for limited numerical scales can be obviously seen as non-zonal. LNS is announced to identify resolvable and unresolvable fractions of the turbulent kinetic energy. The switching from RANS to LES is performed by a factor appearing in the formulation of the eddy viscosity ν_t and expressed by the comparison between the product of the length and velocity scales of RANS and LES. Contrarily to DES, the grid has no influence on the interface position. A zonal approach is used for example by Schlüter et al. [36]. Here the method does not concentrate on near-wall or outer regions but divides the flow domain according to RANS or LES advantages. Two separate solvers (one LES solver and one RANS solver) running simultaneously and exchanging information at the interfaces compute the flow. In this case, the problem of performing a realtime communication between the two codes arises. Another option is to implement both modes in a single code. Several of these kinds of zonal approaches were proposed. e.g., von Terzi et al. [54] suggested a procedure in which the LES region is first followed by a 3D URANS region and then finally switches to 2D RANS. However, none of these various techniques showed an overall superiority over the others and the question *zonal* or *non-zonal* is still open and might remain open depending on the flow problem considered.

The main questions concerning hybrid techniques generally arise when considering the interface between LES and RANS. First the case in which RANS is applied in the near-wall region and LES in the core region is addressed. Different studies mentioned above tend to prove that hybrid LES–RANS simulations can provide good results without special LES–RANS interface treatment. Nevertheless, the characteristics of how turbulence is tackled in both regions are by definition different. Moreover, unphysical behavior encountered around the interface when simulating wall-bounded flows such as the plane channel flow lead to the assumption that an interface treatment could improve the predictions of hybrid approaches. Indeed, the literature [3,10,30,50] provides a large range of questions about this topic. The location and definition of the interface as well as the nature of the matching conditions should be mentioned here. Another important point is the blending of the filtering method applied in LES with RANS models using time-averaged data. In other words, which response does the RANS model give when fed with an unsteady field provided by LES and vice versa? For Temmerman et al. [50] an additional question arises. According to the level of unsteadiness observed in the near-wall region, where the RANS model operates, are the assumptions on which the RANS models are closed still valid? A

related contradiction pointed out by several groups [3,10,21,30,36,50] is the use of statistical information coming from the RANS region whereas LES requires small-scale motions close to the interface in order to sustain the turbulence dynamics.

Concerning the interface influence Temmerman et al. [50] obtained better predictions of the log-law region when the interface is located remotely from the wall and additionally this influence is found to be weakened. However, this conclusion is in contradiction to the observation that less realistic turbulent features are obtained when the RANS model spreads away from the wall. This point has also been observed by Piomelli et al. [30]. As noticed by numerous researchers, an unphysical step named "DES buffer layer" by Piomelli et al., appears in the prediction of the mean streamwise velocity. This behavior originates from a mismatch of the different scales involved in both regions: long unphysical wall streaks in the RANS region (super-streaks) but shorter scales in the LES region. The "DES buffer layer" occurs in those regions where these short scales are generated. By decreasing the RANS region, the extent of the long streaks is reduced and structures characterized by shorter wavelengths and time-scales are noticed in the near-wall region. Nevertheless, the "DES buffer layer" still exists despite the generation of short-scale fluctuations. Piomelli et al. [30] concluded that the "coupling between the physical picture of the LES–RANS transition region and the mean velocity profile may be weaker than conjectured". Following a suggestion of Baggett [1] that a "stochastic backscatter model has the effect of breaking up the super-streaks and thus introduce a de-correlation of the velocity allowing a more rapid formation of Reynolds-stress generating eddies", Piomelli et al. [30] applied in the region below the interface (RANS region) a model of this type representing the effect of the subgrid scales. This implementation resulted in a break-up the long unphysical streaks, the generation of smaller scales near the interface as well as the elimination of the "DES buffer layer". It was found that the backscatter model inputs a substantial amount of turbulent kinetic energy at the interface as well as introduces vorticity. Thus the model modifies the mean velocity profile by "generating rotational motions that are effective in supporting Reynolds shear stress". As acknowledged by the authors [30], however, the technique used is based on a backscatter model without physical justification. Further investigations are required.

Temmerman et al. [50] also proposed a correction of the RANS model, which is announced to be "similar in spirit but procedurally simpler and more natural" than the method of Piomelli et al. The response of a near-wall RANS model fed with an unsteady motion extracted from a wall-resolved LES was studied. The conclusion is that the RANS model reproduced realistic turbulent features at least for larger scales. These results could be seen as positive. However, it shows that the "total (modeled + resolved) second moments" provided by the RANS model is larger than in LES, leading to a discontinuity in the turbulent kinetic energy and total eddy viscosity. Indeed the resolved contributions of both RANS and LES modes are comparable whereas RANS provides a larger modeled contribution than LES. For this purpose, Temmerman et al. [50] corrected the near-wall RANS model in order to obtain an eddy-viscosity continuity between both RANS and LES. This modification was tested on a plane channel flow as well as on a periodic hill flow yielding good results in both cases. Nevertheless, this technique has to be further studied to confirm these results and test its generality. Moreover, the modification suggested does not solve the problem of long unphysical wall streaks in the near-wall region.

A commonly studied strategy aimed at improving the RANS-LES transition and providing LES with relevant turbulent structures is to add reconstructed turbulent fluctuations at the interface. Davidson et al. [10] proposed a treatment of this type. Instantaneous turbulent fluctuations taken from a DNS of a channel flow are rescaled and applied at the interface in order to act as a forcing term to drive the momentum equations to "start resolving turbulence". These scaled fluctuations which should be physical in time and length scale related to the ones of the grid cells, are considered by the authors, even if disputable, as "generic". The treatment suggested [10] improved significantly the predictions in the channel flow test case. However, when performed on a 3D hill flow test case, it did not give any significant improvement. The explanation proposed by the authors was that in the second case realistic turbulence was imposed to the hybrid LES–RANS method because of the relative proximity of the inlet from the hill. On the other hand, for the fully developed channel flow the LES only sees poor turbulent features transported from the RANS region to the LES zone. It is assumed that a remotely located inlet in the 3D hill flow case would lead to improvements of the simulation using reconstructed turbulent fluctuations in comparison with standard hybrid LES–RANS strategies.

Batten et al. [3] proposed a treatment of the LES–RANS interface based on a reconstructed, synthetic turbulence field which "preserve a given set of space/time correlations and second moments". Although the study is mentioned to be at a preliminary state, the technique tested on a plane channel flow is found to "preserve the total shear stress across regions into which turbulence is transported via mean convection" and help to sustain the fluctuations in the LES region.

In a non-exhaustive review of strategies in which the RANS mode is allocated to a part of the domain instead of being restricted to the near-wall region, some methods are now briefly mentioned. Schlüter et al. [36] studied a method to "specify meaningful" turbulent inflow conditions in the case that the RANS/LES interface is located in the midst of the computational domain. Here the addition of the "mean flow field of the RANS solution" with "turbulence obtained from a database created by an additional preprocessed LES computation" is used as inflow condition for LES. This method gave interesting results on the test cases investigated, but is not practicable in general.

An alternative is the so-called "random vortex method" proposed by Sergent et al. [38] and Mathey et al. [23] which generates appropriate inflow conditions for LES at the RANS-LES interface.

Finally, another technique, even if not yet used in a hybrid LES–RANS simulation, was introduced by Keating et al. [21] who try to overcome the issue of the "generation of turbulent eddies capable of supporting the Reynolds stresses in the LES region from a smooth RANS field". In order to tackle this problem, Keating et al. uses synthetic turbulence [3] coupled with a controlled forcing term added to the wall-normal momentum equation that amplifies the velocity fluctuations in that direction. This method is found by the authors to be effective in generating realistic turbulence. Nevertheless, it has the disadvantage to be computationally expensive.

In the present work, a non-zonal hybrid LES–RANS approach relying on a unique modeling concept is suggested. In both modes a transport equation for the turbulent kinetic energy is solved, either for the trace of the modeled stresses in the viscosity-affected near-wall RANS zone or for the subgrid-scale contributions in the LES zone. The closure is completed by algebraic relations for the length scales in the near-wall region and the assumption that the length scale in LES can be represented by the filter width. The simulations assessing the hybrid LES–RANS approach are performed on the "flow over periodic hills" test case including pressure-induced flow separation and subsequent reattachment [24] as well as on the plane channel flow test case. The plane channel flow is a challenging and common test case for hybrid LES–RANS simulations [3,11,27,50]. Indeed the flow is dependent on the near-wall region. On the other hand the periodic hill flow was found to be difficult for a wide range of RANS models [20,22]. This type of closures fails in the estimation of the reattachment location since they cannot capture the large-scale dynamics in the separated shear layer.

The paper is organized as follows. First, the SGS and RANS models are presented in Sects. 2.1 and 2.2 as well as the interface criteria (Sect. 2.3). Section 3 will propose an overview of the numerical solution method applied. In the subsequent paragraph the geometry and the details of the flow configuration are defined, including details on the grids and boundary conditions used. First results are presented in Sect. 5. Afterwards, different modifications performed on the RANS model are mentioned (Sect. 6). Finally, the improved results are presented and analyzed.

2 Hybrid LES–RANS method

In the present study a non-zonal approach is selected signifying that the LES and RANS domains are not known beforehand but dynamically computed within the simulation. Besides, the LES–RANS interface is based on physical quantities and not on numerical ones, such as the grid resolution. Thus, the predefinition of these zones is avoided for unknown flows. The method suggested could be qualified as a *natural* hybrid method combining RANS and LES. This means that near solid boundaries the governing equations *work* in RANS mode, i.e., the turbulent stresses are modeled with the help of a statistical turbulence model. Furthermore, unsteady attached vortical structures should not be resolved directly. Far from solid boundaries, the method *switches* to LES mode. From the physical point of view, it means resolving all large-scale vortical structures and modeling the small eddies based on a subgrid-scale model, which can be formally similar to a statistical turbulence model. From the numerical point of view, one has to deal with unsteady fields of pressure and velocity in this mode. However, the flow is not explicitly subdivided into two zones, and thus the computational domain contains no explicit boundaries or interfaces between the two modes of operation. Instead, the boundary is dynamically determined by the code and flow characteristics.

Another important issue is the question of suitable models for such hybrid methods. For the non-zonal methodology a unique modeling strategy as used by DES has certain advantages. Two of such benefits are that the use of boundary conditions (for $k, \epsilon, \ldots$) at the LES–RANS interface can be avoided and the switching between RANS and LES can be performed in a simple manner. In the context of eddy-viscosity models for RANS, a two-equation model is a natural choice since one transport equation is solved for the velocity scale and one for the length scale. LES zero- or one-equation models are more obvious since the length scale is

naturally given by the filter width Δ. Consequently, these facts are in contradiction to a unique model. However, if the near-wall region is the main target for RANS, the length scale can be prescribed by an algebraic relation. This leads to a one-equation model for both zones.

This one-equation modeling methodology has already been applied (e.g., Davidson et al. [10,11] and Temmerman et al. [50], the latter using the SGS model of Yoshizawa [57] combined with the one-equation model of Wolfshtein (RANS) [56]). However, the choice of one-equation models diverges in the present investigation. For the near-wall RANS region the model adopted in the present study is based on the two-layer approach proposed by Rodi et al. [33]. They used a one-equation model for the viscosity-affected near-wall layer and combined it with a standard k-ϵ model for the outer region to a two-layer RANS model. Hence the formulation for the inner layer is taken over, but the outer region is basically replaced by LES. The resulting unique model consists of a transport equation for the modeled turbulent kinetic energy k_{mod} in RANS mode and the subgrid-scale (SGS) turbulent kinetic energy k_{sgs} in LES mode, respectively. Both models are then distinguished by their definitions of the dissipation rate ϵ of the turbulent kinetic energy k $(= 1/2 \cdot (\overline{u_i' u_i'}))$ and the eddy viscosity ν_t (Sects. 2.1 and 2.2).

The general transport equation for k reads

$$\frac{\partial k}{\partial t} + \overline{U_j}\frac{\partial k}{\partial x_j} = \frac{\partial}{\partial x_j}\left[(\nu + \frac{\nu_t}{\sigma_k})\frac{\partial k}{\partial x_j}\right] + \underbrace{\nu_t\left(\frac{\partial \overline{U_i}}{\partial x_j} + \frac{\partial \overline{U_j}}{\partial x_i}\right)\frac{\partial \overline{U_i}}{\partial x_j}}_{\mathcal{P}} - \epsilon. \tag{1}$$

$\overline{U_i}$ has to be understood as time-averaged U_i in RANS mode and filtered U_i in LES mode. This equation has to be closed by appropriate modeling assumptions for ϵ and ν_t, which are treated differently in the LES and RANS zones, respectively.

2.1 SGS model for the hybrid technique

Before applying the present hybrid LES–RANS technique, it is necessary to agree on a subgrid-scale model for the LES mode. The basic idea is to employ a similar one-equation model for k in RANS and LES modes. Consequently, for LES the transport equation (1) is taken into account in order to describe the subgrid-scale turbulent kinetic energy k_{sgs}. The standard formulations of ϵ and ν_t for the SGS one-equation model [31,34, 37,57] are defined as

$$\nu_t = C_\mu \cdot k_{\mathrm{sgs}}^{1/2} \cdot \Delta, \tag{2}$$

$$\epsilon = C_d \cdot k_{\mathrm{sgs}}^{3/2}/\Delta, \tag{3}$$

$$\Delta = (\Delta x \cdot \Delta y \cdot \Delta z)^{1/3}. \tag{4}$$

Thus, the decision has to be taken on the value of the constants C_d and C_μ used for the definition of ϵ and ν_t, respectively. For this purpose several sets of constants have been tested on the plane channel flow test case. These tests have been performed applying constants suggested by Schumann [37], Yoshizawa [57] and Pope [31] relying on the Kolmogorov energy spectrum as well as a model proposed by Sagaut [34] also based on the energy spectrum but using spectral methods such as EDQNM (eddy-damped quasi-normal Markovian) theory for the adjustment of the constants. All models have given similar results. Therefore, it has been decided that the main set should be $C_\mu = 0.05$ and $C_d = 1.0$ as proposed by Schumann. However, the LES models have to be checked for more complex flow situations and under varying grid resolutions.

2.2 RANS model for the hybrid technique

The next step is to define the RANS model which is applied in the hybrid LES–RANS technique. The objective is to use a simple model based on the turbulent kinetic energy and due to the restricted area in which the model operates, especially designed for the viscosity-affected near-wall region. Moreover, it is preferred to avoid the disadvantage of using damping functions, which are normally required for the length scale l_μ and the dissipation length l_ϵ. The following model meets these mentioned key points and to the authors' knowledge has not been applied in an hybrid method yet.

In order to improve the quality of the prediction of the RANS technique, Rodi et al. [33] formulated a one-equation near-wall turbulence model. Its particularity is the use of the wall-normal velocity fluctuations $\overline{v'^2}$ as velocity scale instead of k ($= k_{\mathrm{mod}}$). As a consequence only one damping function is required. The formulation shown below is the original model suggested by Rodi et al. [33], which was combined with the k-ϵ model in the outer region to a two-layer RANS approach. The empirical relations for ν_t and $\overline{v'^2}$ of the near-wall RANS model read

$$\nu_t = (\overline{v'^2})^{1/2} \cdot l_{\mu,v}, \tag{5}$$

$$l_{\mu,v} = C_{l,\mu} \cdot y \quad \text{with } C_{l,\mu} = 0.33, \tag{6}$$

$$\overline{v'^2}/k_{\mathrm{mod}} = 4.65 \times 10^{-5} y^{*2} + 4.00 \times 10^{-4} y^* \quad \text{for } y^* \leq 60, \tag{7}$$

$$y^* = k_{\mathrm{mod}}^{1/2} \cdot y/\nu. \tag{8}$$

Here y and y^* denote the wall-normal distance and its scaled variant, respectively. The empirical relations for ϵ are given by

$$\epsilon = (\overline{v'^2})^{1/2} \cdot k_{\mathrm{mod}}/l_{\epsilon,v}, \tag{9}$$

$$l_{\epsilon,v} = 1.3y/\left(1 + 2.12\frac{\nu}{(\overline{v'^2})^{1/2} y}\right). \tag{10}$$

As shown by Rodi et al. [33] and originally introduced by Durbin [13], for the near-wall region (RANS mode) the wall-normal velocity fluctuations $(\overline{v'^2})^{1/2}$ are better suited to characterize the turbulent motion than k_{mod} as characteristic velocity scale. The length scale $l_{\mu,v}$ appearing in the eddy-viscosity relation ν_t, generally defined as $\left[\nu_t = C_\mu \cdot k^{1/2} l_\mu\right]$ in a one-equation model now scales linearly with the wall distance y and needs no damping function anymore. Indeed the eddy-viscosity reduction in the vicinity of the wall is an effect of the decreasing v' fluctuations rather than a viscous one and hence is naturally taken into account. The dissipation length $l_{\epsilon,v}$ used to define the dissipation rate ϵ, which usually reads $\left[\epsilon = C_d \cdot k^{3/2}/l_\epsilon\right]$ in a one-equation model, also scales linearly near the wall. Only in the immediate vicinity of the wall the distribution must be modified to yield the correct behavior of $\epsilon \sim y^0$ as y goes to zero. In order to apply $(\overline{v'^2})^{1/2}$ as the velocity scale in the model, Rodi et al. provided (7) to relate the wall-normal velocity fluctuations to the distribution of k (equivalent to k_{mod} in RANS mode) so that the transport equation does not have to be adjusted. Instead of using the scaled variable y^+, formulated with the wall-shear stress velocity u_τ, they have introduced y^*, which allows the model to be applied in separated flows, for which τ_w is zero or negative. This formulation of $\overline{v'^2}$ is valid up to $y^* \approx 60$, which according to DNS results [26] corresponds to $y^+ \approx 30$ for the channel flow test case. Finally, one can notice that the constant C_μ usually used in the eddy-viscosity definition is now included in the eddy-viscosity length scale relation.

2.3 LES–RANS interface

Regarding the LES–RANS interface, two critical points are how to combine both techniques and how to choose a criterion to shift from RANS to LES. In the present study a non-zonal approach involving an interface treatment without synthetic or reconstructed turbulence is preferred as one of the objectives at this phase of the investigation is to assess the suggested method in its simplest form prior to further developments. The introduction of such mechanisms (synthetic and reconstructed turbulence) or the derivation of a solution for the "DES buffer layer" is the subject of the ensuing stages of the investigation.

In Rodi et al.'s two-layer approach [33], the ratio of the eddy viscosity to the molecular viscosity ν_t/ν is employed as switching criterion. In the vicinity of the wall, the one-equation near-wall turbulence model is applied until the ratio ν_t/ν reaches a fixed value C_{switch}. Then the outer model is used. In order to keep the requirement $y^* \leq 60$, C_{switch} was set to 16 by Rodi et al. [33]. In the hybrid LES–RANS technique this value cannot be applied as ν_t in the LES mode is much lower than ν_t in the RANS mode. Furthermore, once the critical value of ν_t defined as $\left[\nu_{t,\mathrm{crit}} = \nu \cdot C_{\mathrm{switch}}\right]$ is attained in the RANS mode, ν_t strongly decreases in the LES mode and hence fall below the critical value $\nu_{t,\mathrm{crit}}$ again. Then the entire simulation is treated in RANS which is not desired. The suitable ratio for the LES–RANS switch is found for $C_{\mathrm{switch}} < 1$. However, this criterion does not offer suitable results. Although the simulation shifts from RANS to LES at a reasonable

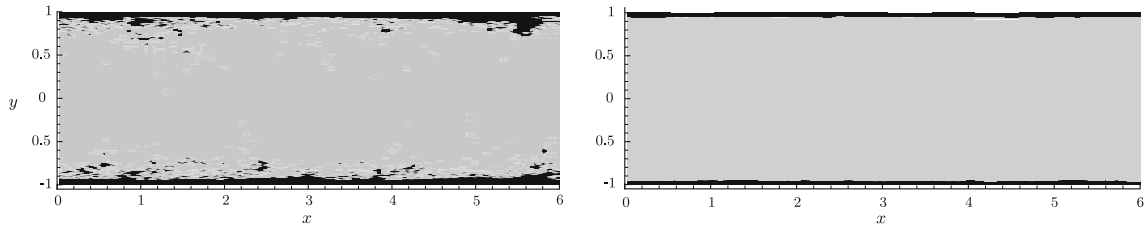

Fig. 1 Channel flow test case at $Re_\tau = 590$. RANS-LES domain layout for *hybrid versions A* (*left*) and *B* (*right*). RANS domain *black zone*. LES domain *grey zone*

distance from the wall, the technique switches back from LES to RANS in the core of the domain when ν_t decreases and finally reaches the critical ratio $\nu_{t,\mathrm{crit}}$. Therefore, this criterion has been abandoned. As a remedy for the present hybrid LES–RANS technique, different dynamic switching criteria have been tested to define the interface between RANS and LES.

Criterion y^* based on the modeled turbulent kinetic energy k_{mod}: *hybrid version A*

The objective of the method is to use a dynamic interface criterion based on physical parameters (mainly turbulent parameters). Therefore, the idea is to introduce the turbulent kinetic energy k in this criterion. It has been decided to apply the dimensionless value y^* defined by $\left[y^* = k^{1/2} \cdot y/\nu\right]$ as switching condition. Moreover, y^* is already computed within the one-equation RANS model of Rodi et al. and used in the algebraic expression of $(\overline{v'^2})$. y^* has also the advantage to be applicable in separated flow configurations. By applying this criterion the method is supposed to be able to determine automatically the zones of high or low turbulent intensity in the near-wall region through the use of k. The wall distance y is assumed to prevent the method from switching back to RANS in the core LES region of the domain. The interface is defined as

$$\begin{cases} y^* \le C_{\mathrm{switch},y^*} \Longrightarrow \text{RANS mode} \\ y^* > C_{\mathrm{switch},y^*} \Longrightarrow \text{LES mode} \\ \\ \text{with } y^* = k_{\mathrm{mod}}^{1/2} \cdot y/\nu \quad \text{and} \quad C_{\mathrm{switch},y^*} = 60 \end{cases} \tag{11}$$

Thus, the dynamic criterion y^* based on k_{mod} is applied to define the LES–RANS interface. As no averaging is required in the determination of the interface, the method is self-starting (in time). Below $y^* = 60$ (validity restriction of $(\overline{v'^2})$) the simulation is performed in RANS mode. However, this condition gives, in the channel flow test case, no sharply delimited LES–RANS regions (see Fig. 1 and the following criterion y_2^* for explanation).

Criterion y_2^* based on the total turbulent kinetic energy k_{tot}: *hybrid version B*

In order to get over the last remark, the new criterion y_2^* is introduced, which is defined as follows $\left[y_2^* = k_{\mathrm{tot}}^{1/2} \cdot y/\nu\right]$. Hence y_2^* is a modification of y^* by replacing k_{mod} by k_{tot} described by $\left[k_{\mathrm{tot}} = k_{\mathrm{mod}} + \overline{k}_{\mathrm{res}}\right]$. Here k_{tot} and k_{res} denote the total and the resolved turbulent kinetic energy, respectively. $\overline{k}_{\mathrm{res}}$ is defined as $\left[1/2 \cdot ((\overline{u_i' u_i'})_{\mathrm{res}})\right]$ where $(\overline{u_i' u_i'})_{\mathrm{res}}$ is averaged in time and homogeneous directions (if available). A drawback of this formulation is that the time averaging makes the interface type *B* not fully self-starting in opposition to *A*. Furthermore, time averaging is not always possible (e.g., for time-dependent boundary conditions). Then other techniques such as a recursive digital low-pass filter [6] or an averaging procedure along trajectories of particles [25] can be envisaged. Both methods mentioned above are notably applied within the dynamic SGS model procedure in order to solve equivalent problem.

After assessing the switching criterion based on y^*, it has been seen that no clearly delimited RANS and LES regions are obtained. This fact is a consequence of using k_{mod} in the formulation of y^*. As can be seen in Fig. 2 (left) based on the averaged values, $\overline{k}_{\mathrm{mod}}$ closely follows the curve k_{crit}, which is defined

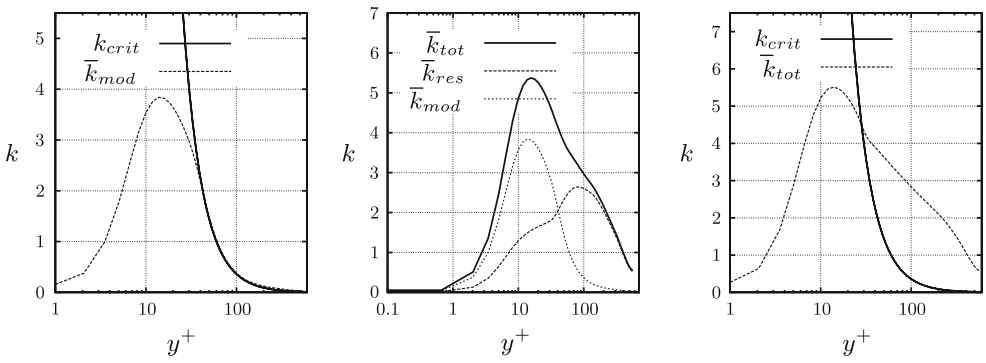

Fig. 2 Channel flow test case at $Re_\tau = 590$. Behavior of $\overline{k}_{\text{mod}}$ in comparison with k_{crit} (*left*). $\overline{k}_{\text{mod}}$, $\overline{k}_{\text{res}}$ and $\overline{k}_{\text{tot}}$ of *hybrid version A* (*center*). Behavior of $\overline{k}_{\text{tot}}$ in comparison with k_{crit} in *hybrid version B* (*right*)

as $\left[k_{\text{crit}} = (C_{\text{switch}} \cdot \nu/y)^2\right]$ and represents the limit between RANS and LES ($k_{\text{mod}} \leq k_{\text{crit}}$ meaning RANS mode). Thus, it is obvious that the instantaneous k_{mod} used in *hybrid version A* fluctuates around the curve k_{crit}, which creates these mixed LES–RANS zones. As a remedy the presence of resolved turbulent scales in the RANS region (Fig. 2, center) is accounted for. Indeed, in steady RANS k_{mod} is expected to correspond to k_{tot} and thus k_{res} should be zero. That is not the case here. Since it operates as an unsteady RANS (URANS), also the RANS mode resolves some turbulent scales. Thus, k_{mod} in y^* is replaced by k_{tot}, which gives a higher value of k used in the switching criterion. Although k_{tot} is calculated with the instantaneous k_{mod} in order to keep the dynamic nature for the interface type *B*, the resolved contribution is averaged. Indeed, the purpose here is to add a contribution to k_{mod} in order to remove the RANS islands. To use the instantaneous distribution of k_{res} here is critical since the fluctuating character of k_{res} may not completely cancel out the problem. Thus, $\overline{k}_{\text{res}}$ is preferred. Moreover, an additional feature of applying $\overline{k}_{\text{res}}$ is the smoothness of the interface obtained as shown for the hill flow test case (Sect. 7.4).

Hence, y_2^* provides two distinct RANS and LES domains. The effect of this modification is observed in Figs. 1 and 2 (right). Unlike y^*, y_2^* provides a sharp interface between RANS and LES ($k_{\text{crit}} \geq \overline{k}_{\text{tot}} \Longrightarrow$ RANS and $k_{\text{crit}} < \overline{k}_{\text{tot}} \Longrightarrow$ LES). Thus, the interface is defined as

$$\begin{cases} y_2^* \leq C_{\text{switch},y_2^*} \Longrightarrow \text{RANS mode} \\ y_2^* > C_{\text{switch},y_2^*} \Longrightarrow \text{LES mode} \\ \\ \text{with } y_2^* = k_{\text{tot}}^{1/2} \cdot y/\nu \quad \text{and} \quad C_{\text{switch},y_2^*} = 60 \end{cases} \tag{12}$$

It has to be noticed that the condition $y_2^* \leq 60$ always keeps the requirement $y^* \leq 60$ and that y^* is kept in the formulation of the model, i.e., (7)–(8). The LES–RANS interface using $y_2^* \leq 60$ as criterion is located at $y^+ \approx 30$ for the plane channel flow.

Criterion y^* with sharp interface treatment: *hybrid version Asi*

The computations performed with the interface criterion based on y_2^* showed that the gain of a clear interface is accompanied by a large reduction of the RANS region (Fig. 1) as a result of $y_2^* > y^*$. Although C_{switch,y_2^*} can be increased to values larger than 60, the prediction beforehand of a concrete limiting value is not possible. Thus, $C_{\text{switch},y_2^*} = 60$ is kept, which reduces the RANS region significantly. In order to retain a RANS region of similar extension as *hybrid version A* but in conjunction with a sharp interface, a new approach is implemented. This converts all undesired RANS islands back to LES and provides a sharp interface when the *hybrid version A* is applied. The procedure is as follows. A RANS control volume is converted to LES if among its six neighboring control volumes (CVs sharing a common surface) the CV characterized by the lowest wall distance is treated in LES mode (see Fig. 3 for explanation).

This treatment of the interface will provide useful outcomes to check whether the RANS islands mentioned for the *hybrid version A* influence the results or not. The comparison between the treatment *A* and *Asi* is presented for the hill flow test case (Sect. 7.4; Fig. 14) for which the interface criteria are further discussed.

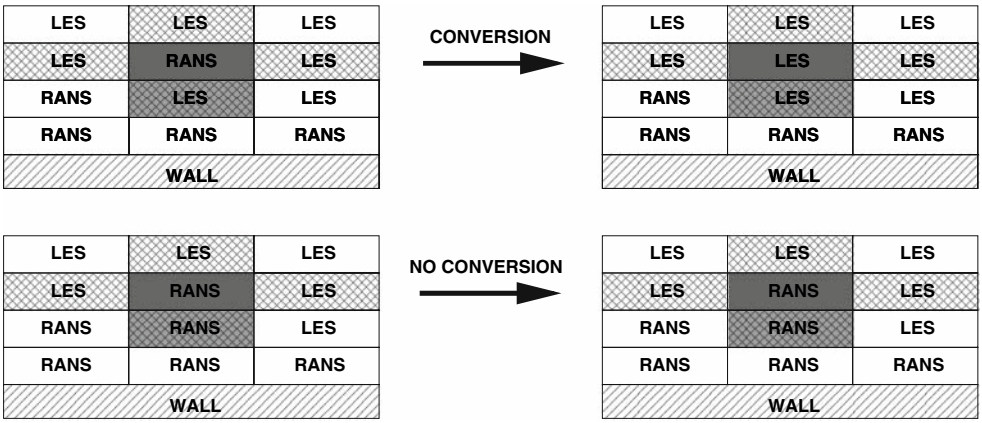

Fig. 3 Conversion of a RANS CV to LES (*top*). The RANS CV is selected (*dark grey*). The neighboring CVs are distinguished by the crossed patterns. The neighboring CV characterized by the lowest wall-distance (*bright grey with crossed patterns*) is selected for testing. If this CV is in LES mode, the dark RANS CV is converted to LES. The opposite case is shown below

3 Numerical methodology

All simulations were performed with the LES code $\mathcal{LESOCC}$, used for the solution of the filtered Navier–Stokes equations. This is a 3D finite-volume solver for arbitrary non-orthogonal and non-staggered (block-structured) grids [4–6]. The spatial discretization of all fluxes is based on a central scheme of second-order accuracy. A low-storage multi-stage Runge–Kutta method (second-order accurate) is applied for time-marching the momentum equations in the first step of the predictor–corrector method. Subsequently, a Poisson equation is solved for the pressure correction in the corrector step leading to a divergence-free velocity field. The additional transport equation (1) for the turbulent kinetic energy is discretized with the same scheme. Pressure–velocity coupling is achieved on the colocated grid using the momentum interpolation technique suggested by Rhie and Chow [32]. By applying an incomplete lower–upper decomposition, the Poisson equation is iteratively solved. Beside the hybrid approach described above, different SGS models for LES are implemented (Smagorinsky model [40] and dynamic Smagorinsky model [15]) as well as DES (Spalart–Allmaras model [41]). These features are used to provide data for comparison with the new hybrid method.

4 Test cases

4.1 Plane channel flow

The first test case used for validating the basic settings and model modifications, is a plane channel flow with periodic boundary condition in streamwise and spanwise directions and no-slip boundary condition at the walls. The dimensions of the computational domain are: 2π (streamwise) $\times$ π (spanwise) $\times$ 2 (wall-normal). The results are compared with DNS data of fully developed plane turbulent channel flow at Reynolds numbers $Re_\tau = 590$ and 2,003 supplied by Moser et al. [26] and Hoyas and Jiménez [18], respectively. The computations are performed on three grids (Table 1). Grid $\mathcal{F}$ (fine) consists in $128 \times 128 \times 128$ control volumes in each directions, which represents a resolution of $\Delta x^+ = O(30)$ (streamwise) and $\Delta z^+ = O(15)$ (spanwise) at $Re_\tau = 590$ but $\Delta x^+ = O(98)$ and $\Delta z^+ = O(49)$ at $Re_\tau = 2,003$. The first grid point (half first cell) is located at position $y^+_{1\text{st pt}} = 0.68$ ($Re_\tau = 590$) and 2.3 ($Re_\tau = 2,003$). A second grid, namely grid $\mathcal{C}1$, much coarser than grid $\mathcal{F}$ and more in adequacy with the objective of the hybrid technique is used for the case $Re_\tau = 590$. Grid $\mathcal{C}1$ contains $64 \times 64 \times 64$ CVs leading to a resolution of $\Delta x^+ = O(60)$ and $\Delta z^+ = O(30)$. The first grid point is located at position $y^+_{1\text{st pt}} = 1.46$. Finally, grid $\mathcal{C}2$ is designed with $64 \times 64 \times 64$ CVs and used at $Re_\tau = 2,003$ leading to the following resolution: $\Delta x^+ = O(196)$, $\Delta z^+ = O(98)$ and $y^+_{1\text{st pt}} = 2.01$. The difference between grids $\mathcal{C}1$ and $\mathcal{C}2$ is found in the wall-normal stretching factor. Tables 1 and 2 summarize the characteristics of the grids and the various computations (hybrid LES–RANS and LES) performed, respectively. Two different sources can be cited defining grid resolution requirements for wall-resolved LES. Piomelli and Chasnov [29] set the limits to $\Delta x^+ = O(50-150)$, $\Delta z^+ = O(15-40)$ and $y^+_{1\text{st pt}} < 2$. According to Sagaut [55], a poor resolution starts with $\Delta x^+ \geq O(100)$ and $\Delta z^+ \geq O(30)$. Thus,

Table 1 Grid resolutions for the channel flow test case

Grid	Re_τ	Re_b	$N_x \times N_y \times N_z$	Δx^+	Δz^+	$y^+_{\text{1st pt}}$	Stretching factor
$\mathcal{F}$	590	10,935	$128 \times 128 \times 128$	30	15	0.68	1.05
$\mathcal{F}$	2,003	48,505	$128 \times 128 \times 128$	98	49	2.3	1.05
$\mathcal{C}1$	590	10,935	$64 \times 64 \times 64$	60	30	1.46	1.1
$\mathcal{C}2$	2,003	48,505	$64 \times 64 \times 64$	196	98	2.01	1.143

Re_b Reynolds number based on the bulk velocity; N_x, N_y, N_z number of control volumes in streamwise, wall-normal and spanwise directions, respectively; Δx^+, Δz^+ and $y^+_{\text{1st pt}}$ resolution in streamwise, spanwise and wall-normal directions, respectively Stretching factor in the wall-normal direction

Table 2 Channel flow simulations

Sect.	Case	Grid	Re_τ	Sim.	Models	Const.	Int.	Funct.	t_a/t_z
Section 5	A	$\mathcal{F}$	590	Hyb.	NWOER/OEsch	orig.	A	–	29.93
	B	$\mathcal{F}$					B	–	14.01
	LES1	$\mathcal{C}1$		LES	Smag.	–	–	–	31.82
	A	$\mathcal{F}$					A	–	27.04
	A	$\mathcal{C}1$					A	–	19.10
Section 7.1.1	Asi	$\mathcal{F}$	590	Hyb.	NWOER/OEsch	mod.	Asi	–	23.89
	Asi	$\mathcal{C}1$					Asi	–	19.10
	B	$\mathcal{F}$					B	–	17.51
	B	$\mathcal{C}1$					B	–	19.10
	LES2	$\mathcal{F}$		LES	OEsch	–	–	–	28.96
	LES3	$\mathcal{F}$		LES	Smag.	–	–	–	36.29
	Afdyn	$\mathcal{F}$					A	fdyn	24.89
	Afdyn	$\mathcal{C}1$					A	fdyn	20.16
Section 7.1.2	Asidyn	$\mathcal{F}$	590				Asi	fdyn	23.50
	Asidyn	$\mathcal{C}1$		Hyb.	NWOER/OEsch	mod.	Asi	fdyn	28.53
	Bf	$\mathcal{F}$					B	f	15.70
	Bfdyn	$\mathcal{F}$					B	fdyn	16.81
	Bfdyn	$\mathcal{C}1$					B	fdyn	20.40
	LES4	$\mathcal{C}2$		LES	Smag.	–	–	–	23.87
	A	$\mathcal{F}$					A	–	20.54
	A	$\mathcal{C}2$					A	–	17.17
Section 7.2	Asi	$\mathcal{F}$	2,003	Hyb.	NWOER/OEsch	mod.	Asi	–	19.19
	Asi	$\mathcal{C}2$					Asi	–	17.91
	B	$\mathcal{F}$					B	–	19.01
	B	$\mathcal{C}2$					B	–	17.24

Sect section in which the simulation is studied; *Sim* simulation type; *Hyb* hybrid LES–RANS; *Smag* Smagorinsky SGS model; *NWOER* near-wall one-equation model of Rodi et al.; *OEsch* SGS one-equation model of Schumann; *Const* set of constants in the RANS model of Rodi et al. (Sect. 6.1); *orig* original set of constants; *mod* modified set of constants; *Int* interface type; *funct* type of compensating function (Sect. 6.2); f empirical compensating function; *fdyn* dynamic compensating function; t_a averaging time; t_z flow-through time

the grids $\mathcal{F}$ (at $Re_\tau = 2,003$) and especially $\mathcal{C}2$ do not fulfill these requirements but enter in the range of resolution aimed by hybrid LES–RANS simulations.

4.2 Periodic hill flow

The hill flow configuration was a test case at the "ERCOFTAC/IAHR/COST Workshop on Refined Turbulence Modeling" in 2001 [20] and 2002 [22]. Moreover, it has been extensively studied for DES assessments by Breuer et al. [7,8], Jaffrézic et al. [19] and Šarić et al. [35]. The basic idea was to set up a geometrical simple test case which allows one to perform basic investigations based on a complex flow, including pressure-induced separation and subsequent reattachment. Figure 4 shows a sketch of the configuration. The dimensions of the domain are: $L_x = 9.0h$ (streamwise), $L_y = 3.035h$ (wall-normal) and $L_z = 4.5h$ (spanwise) [24]. The flow is assumed to be periodic in the streamwise direction.

As no DNS was performed at the Reynolds number of $Re_b = 10,595$ (based on the bulk velocity U_b and the hill height h), the solution used for evaluating the hybrid simulations is a highly wall-resolved LES [7,9] consisting of a block-structured curvilinear grid with about 12.4×10^6 control volumes using the finite-volume

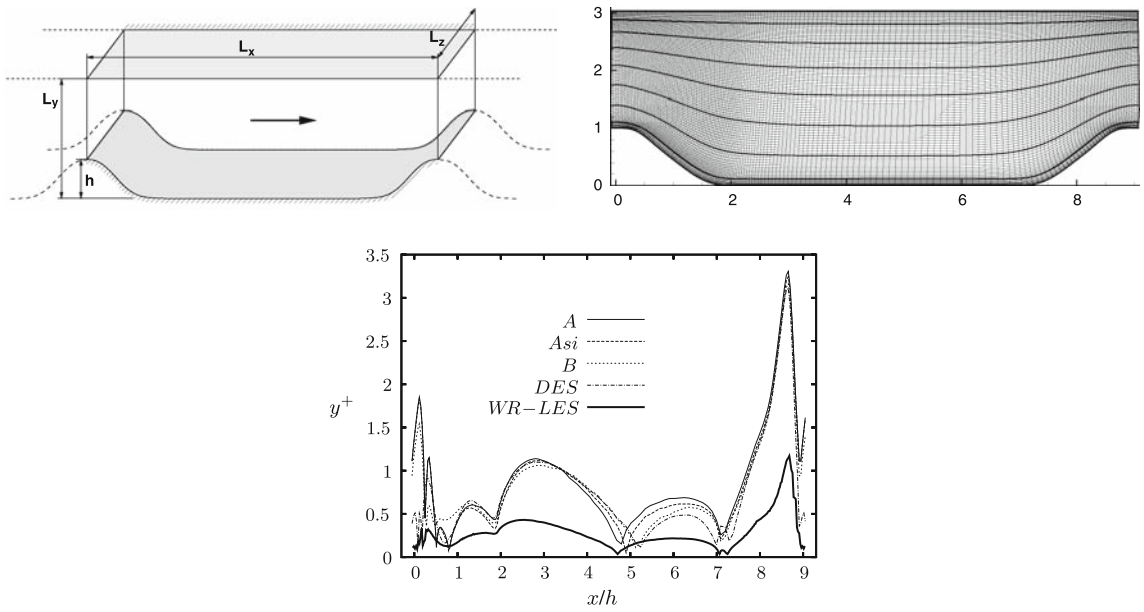

Fig. 4 Periodic hill flow test case. 3D sketch (*upper left*). *x*–*y* sketch of the grid (*upper right*). y^+ distribution at the lower wall (*lower*) for three hybrid simulations and a DES on the coarse grid as well as the wall-resolved LES prediction [7,9]

code $\mathcal{LESOCC}$ (Sect. 3). Some details about this solution denoted in the following WR-LES should be provided here. The grid points are clustered in the vicinity of the lower and upper walls as well as in the region where the free shear layer appears. The resolution of the near-wall region is described by the distribution of non-dimensional y^+ values defined as $\left[y^+ = \Delta y_{cc} \cdot u_\tau / \nu\right]$ where Δy_{cc} denotes the distance from the wall of the cell center (Fig. 4). On the lower wall, y^+ is below 0.45 with a mean value of about 0.2 except at the windward side of the hill. Here the largest values of the wall shear stress are observed and y^+ reaches its maximum of about 1.2. Regarding the wall-normal resolution the grid satisfies the requirements of a wall-resolved LES prediction. Compared to previous studies [14,49] who employed in their highly resolved simulations a curvilinear grid with about 4.6×10^6 CVs, especially the number of grid points in the wall-normal direction is increased in the present WR-LES solution. Furthermore, the upper wall is also resolved by a DNS-like representation ($y^+ \leq 0.95$). Thus, in contrast to [14,49] the application of a wall function is avoided. Overall the grid is much finer than in [14,49]. For example, the cell sizes at the hill crest, which is a key region for the periodic hill flow, are in the current case $\Delta x_{\text{crest}}/h = 0.026$ and $\Delta y_{\text{crest}}/h = 2.0 \times 10^{-3}$ whereas the corresponding values in [14,49] are $\Delta x_{\text{crest}}/h = 0.032$ and $\Delta y_{\text{crest}}/h = 3.3 \times 10^{-3}$, respectively. Owing to the increased resolution in streamwise and spanwise directions the cell sizes expressed in wall units are below $\Delta x^+ = 20$ and $\Delta z^+ = 9$ and thus lower than in [14,49] and substantially lower than the recommendations for wall-resolved LES given by Piomelli and Chasnov [29]. That also holds at the windward slope of the hill where the largest shear stresses are found. Concerning the subgrid-scale modeling, the dynamic Smagorinsky eddy-viscosity model [15] is applied. The boundary conditions are as follows: no-slip condition at the walls and periodic boundary condition in spanwise and streamwise directions (fixed mass flow rate). To gather reliable statistical data the flow has been averaged in time (dimensionless averaging time $T_{\text{avg}} = 1277.34$) and along the homogeneous spanwise direction.

Besides, the results obtained by this highly resolved LES have been compared with the highly resolved LES performed by Fröhlich et al. [14]. This assessment has shown a high degree of agreement between both predictions. Moreover, with respect to further studies [7] and a DNS at $Re_b = 5,600$ performed by Peller and Manhart [28], the Reynolds number in the range presently mentioned ($Re_b = 5,600$ to 10, 935) does not have a strong impact on the results. The current highly resolved LES has also been evaluated against the DNS at $Re_b = 5,600$, which has allowed one to observe equivalent results.

In the present investigation, simulations for the hill configuration are performed on a coarse grid (Fig. 4) consisting of $160 \times 100 \times 60$ CVs in streamwise, wall-normal (res.: $\Delta y_{\text{crest}}/h = 5.0 \times 10^{-3}$, 1st CV height) and spanwise directions, respectively. Figure 4 presents the wall-normal resolution through the distribution of y^+ of the various computations performed. It has to be mentioned that this grid was originally designed for DES. The number of grid points in the spanwise direction is moderate so that the RANS region becomes larger. In this configuration the DES technique using the Spalart–Allmaras model switches from RANS to LES at a

Table 3 Periodic hill flow simulations

Case	Sim.	Models	Int.	$N_x \times N_y \times N_z$	Δx^+	Δz^+	$y^+_{1\text{st pt}}$	$\Delta t\, U_b/h$	t_a/t_z
WR-LES	LES	Dyn.	–	$280 \times 220 \times 200$	20	9	0.45	0.0018	141.0
LES	LES	Smag.	–	$160 \times 100 \times 60$	30	30	1.0	0.004	69.6
DES	DES	SA	DES	$160 \times 100 \times 60$	35	33	1.1	0.004	67.3
A	Hyb.	NWOER/OEsch	A	$160 \times 100 \times 60$	35	55	1.8	0.004	91.9
Asi	Hyb.	NWOER/OEsch	Asi	$160 \times 100 \times 60$	35	55	1.8	0.004	56.5
B	Hyb.	NWOER/OEsch	B	$160 \times 100 \times 60$	35	46	1.5	0.004	58.0
Asag	Hyb.	NWOER/OEsag	A	$160 \times 100 \times 60$	35	55	1.8	0.004	92.3
Bsag	Hyb.	NWOER/OEsag	B	$160 \times 100 \times 60$	35	46	1.5	0.004	89.5

WR-LES wall-resolved LES; *Sim* simulation type; *Hyb* hybrid LES–RANS; *Dyn* dynamic Smagorinsky SGS model; *Smag* Smagorinsky SGS model; *NWOER* near-wall one-equation model of Rodi; *OEsch* SGS one-equation model of Schumann; *OEsag* SGS one-equation model of Sagaut; *SA* Spalart–Allmaras model; *Int* interface type; N_x, N_y, N_z number of CVs in streamwise, wall-normal and spanwise directions, respectively; Δx^+, Δz^+ and $y^+_{1\text{st pt}}$ resolution in streamwise, spanwise and wall-normal directions, respectively (these are the maximal values for the range $x/h = 0$ to 8.0. At the windward side of the hill the resolution decreases owing to the increased value of u_τ in this region). $\Delta t\, U_b/h$ normalized time step; t_a averaging time; t_z flow-through time

distance of about 7–9 RANS cells. Table 3 summarizes the characteristics of the simulations carried out on the hill flow test case.

5 First results for the channel flow at $Re_\tau = 590$

The results presented and discussed here concern the hybrid LES–RANS variants *A* and *B* and the fine grid $\mathcal{F}$ only. The objective of this section is to show the deficits of the primary formulation leading to some possible enhancements described in Sect. 6. For the plane channel flow test case (Sect. 4.1) the new hybrid model provides encouraging statistical results, which are displayed in Fig. 5. The switching location of the LES–RANS interface is located at $y^+ \approx 30$ for *hybrid version B*, which is the position expected and estimated based on DNS results. As mentioned in Sect. 2.3, *hybrid version A* does not give a precise interface location.

Compared with the DNS data a higher u_τ value is found in the case of the *hybrid LES–RANS version B* (deviation of +3.4%) whereas *version A* predicts a lower u_τ value (deviation of −2.3%). The streamwise velocity of both hybrid versions show discrepancies in comparison with the DNS reference starting from the core of the RANS region (Fig. 5). Furthermore, U^+ presents an inflection point at the location of the interface ($y^+ \approx 30$), which is the starting location of an unphysical step related to the switching from LES to RANS. This step is often referred to as "DES buffer layer" and generally observed in hybrid simulations, c.f. [27,30]. Nevertheless, the slope of U^+ in the LES zone is recovered with respect to DNS. An inflection point is also observed in the distribution of the root-mean-square of the resolved Reynolds stress $rms(\overline{u'u'})_{\text{res}}$. At the interface one can observe the sudden drop of $\nu^{\text{mod}}_{t,\text{RANS}}$ which passes from a RANS to a LES amplitude at the interface (Fig. 7). Another issue is the overestimation of $\overline{k}_{\text{tot}}$. Both hybrid versions show a similar result despite slightly lower values of $\overline{k}_{\text{mod}}$ by *hybrid version B*. Thus the loss of modeled turbulent kinetic energy is overcompensated by a gain of resolved energy. As expected, the resolved scales do not vanish rapidly at the LES–RANS interface and in the RANS region. The consequence is a high proportion of the resolved field also in the vicinity of the wall (RANS area). Moreover, these results show the influence of the interface criterion. It should be kept in mind that the difference between *hybrid versions A* and *B* is solely found in the switching criterion, whereas the formulation of the RANS model remains the same in both cases. The effect of the interface position on the resolved field is seen in Fig. 5 by noticing the lower proportion of $(\overline{u'_i u'_j})_{\text{res}}$ predicted by the *hybrid version A* compared with *version B*. *Version A* does not switch from RANS to LES at a clear position, however, it is clear that it offers a more extended RANS region. The consequence is the larger proportion of the modeled scales in *version A*. Since the results displayed are not fully satisfactory, two different adjustments of the RANS model are considered in the next section leading to an improvement of the predictions.

6 Modified formulations of the RANS model and resulting enhancements

6.1 Adjustment of the RANS model to a higher Reynolds number

In order to match the objectives of the present study, i.e., to apply LES to high Reynolds number turbulent flows, the model performance has been assessed with data of a more recent, higher Reynolds number ($Re_\tau = 590$)

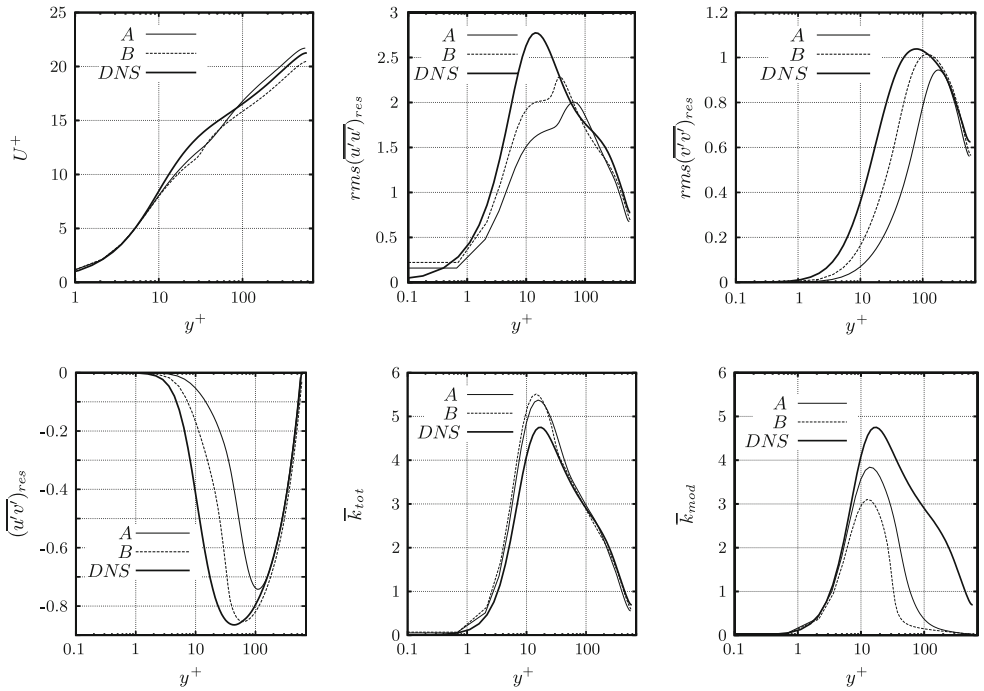

Fig. 5 Channel flow test case at $Re_\tau = 590$, results of *hybrid versions A and B* on grid $\mathcal{F}$. Mean streamwise velocity U^+ (*upper left*). Root-mean-square of the resolved Reynolds stresses $rms(\overline{u'u'}_{\text{res}})$ (*upper center*) and $rms(\overline{v'v'}_{\text{res}})$ (*upper right*). Resolved Reynolds shear stress $\overline{u'v'}_{\text{res}}$ (*lower left*). Turbulent kinetic energies $\overline{k}_{\text{tot}}$ (*lower center*) and $\overline{k}_{\text{mod}}$ (*lower right*). Values scaled with u_τ of each case, respectively. DNS data provided by Moser et al. [26]

DNS of a channel flow (Sect. 4.1). Compared to the reference DNS used originally by Rodi et al. ($Re_\tau = 180$ and 395) to set up the RANS model, the present data are more representative for practical applications since they show a distinct log-region. This study shows that an adjustment of the constants is worth being tested (Fig. 6). An enhanced RANS model using the same architecture but modified constants leading to a much better agreement between the modeled and the real distributions of $(\overline{v'^2}/k)$, $l^+_{\mu,v}$ and $(C_\mu^{1/2} \cdot l^+_{\epsilon,v})$ is defined. The range of interest for the RANS model is approximately $y^+ \leq 30$. The new empirical relations for ν_t and ϵ in this range read

$$\overline{v'^2}/k_{\text{mod}} = 3.55 \times 10^{-5} y^{*2} + 6.50 \times 10^{-4} y^* \quad \text{for } y^* \leq 60 \text{ with } y^* = k^{1/2} \cdot y/\nu, \tag{13}$$

$$C_{l,\mu} = 0.4, \tag{14}$$

$$l_{\epsilon,v} = 1.5y \Big/ \left(1 + 7.65 \frac{\nu}{(\overline{v'^2})^{1/2} y}\right). \tag{15}$$

Now the constant for the length scale is as expected for a log-layer, i.e., the classical von Kármán constant. This new set of constants can be applied to each previously described model version (*A*, *Asi* and *B*). All simulations presented in the following are computed with this new set of constants, whereas the computations performed with the original set by Rodi et al. is called *A0* and *B0*. Moreover, the new set of constants has been freshly assessed with the data of the DNS at $Re_\tau = 2,003$ [18]. It has been observed that the constants could be further adapted, especially for the formulation of $(\overline{v'^2})$. The current expressions for the length scales are still found to be in reasonably good agreement. Thus, a third set of constants has been derived (not shown here). However, tests (not shown here) performed in this direction have not delivered significant differences relatively to the one obtained with the constants presented above.

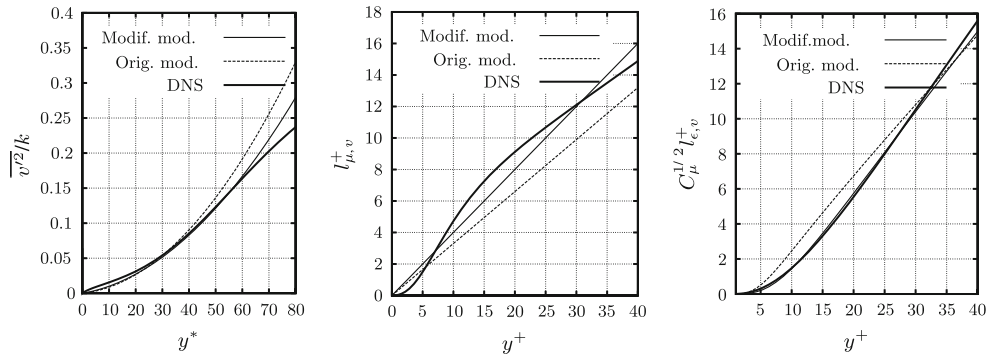

Fig. 6 Channel flow: Distribution of $\overline{v'^2}/k$ (*left*), $l^+_{\mu,v}$ (*center*) and $C_\mu^{1/2} l^+_{\epsilon,v}$ (*right*). Modified model: New model formulation using DNS results of Moser et al. [26] at $Re_\tau = 590$. Original model: Rodi et al.'s formulation [33] based on low-Re results but plotted for DNS results of Moser et al. [26] at $Re_\tau = 590$

6.2 Adjustment of the RANS eddy viscosity

The second modification is a consequence of the presence of resolved turbulent scales in the RANS region. Indeed, as previously mentioned (Sect. 2.3) in steady RANS $(\overline{u'_i u'_j})_{\text{mod}}$ should correspond to $(\overline{u'_i u'_j})_{\text{tot}}$ and the modeled eddy viscosity $\nu^{\text{mod}}_{t,\text{RANS}}$ provided by the model should be the total eddy viscosity $\nu^{\text{tot}}_{t,\text{RANS}}$. Nevertheless, the first campaign of tests carried out on the hybrid approach (Sect. 5) showed a different outcome with the pronounced presence of resolved turbulent scales in the RANS region. Under this condition $\nu^{\text{tot}}_{t,\text{RANS}}$ cannot be longer seen as $\nu^{\text{mod}}_{t,\text{RANS}}$ but represents the sum of $\nu^{\text{mod}}_{t,\text{RANS}}$ and a resolved eddy viscosity $\nu^{\text{res}}_{t,\text{RANS}}$. This $\nu^{\text{res}}_{t,\text{RANS}}$ is obviously not explicitly calculated but depicts the effect of the resolved field. According to this remark the important resolved field contribution might also be taken into account and the formulation of the RANS model, as part of the hybrid approach, can be appropriately adjusted.

In the present RANS model, $\nu^{\text{mod}}_{t,\text{RANS}}$ is calculated based on k_{mod}, which differs from k_{tot} because of the unsteady character of the simulation. Therefore, the resolved field is already implicitly accounted for in the calculation of $\nu^{\text{mod}}_{t,\text{RANS}}$. Nevertheless, the underprediction of U^+ in the channel flow test case (Fig. 5), which can be explained by the overprediction of $\nu^{\text{tot}}_{t,\text{RANS}}$, seems to show that this automatic adjustment of the model is insufficient. This statement is confirmed by Fig. 7 (left), which presents $\nu^{\text{mod}}_{t,\text{RANS}}$. In the RANS region the modeled eddy viscosity $\nu^{\text{mod}}_{t,\text{RANS}}$ closely follows the distribution provided by DNS results derived by the relation $\left[\nu_t = -\overline{u'v'}/(\partial\overline{U}/\partial y)\right]$. However, it should be kept in mind that this reference curve represents the total eddy viscosity $\nu^{\text{tot}}_{t,\text{RANS}}$. Therefore, it is obvious that $\nu^{\text{tot}}_{t,\text{RANS}}$ is overpredicted in the case of the hybrid technique.

Thus, if the assumption that $\nu^{\text{mod}}_{t,\text{RANS}}$ should still be adjusted according to the resolved field, the contribution $(\overline{u'v'})_{\text{res}}$ (Fig. 5, lower left) should be taken into account in the automatic eddy-viscosity adjustment. In order to demonstrate its relevance, the ratio $(\overline{u'v'})_{\text{res}}/(\overline{u'v'})_{\text{tot}}$ versus y_2^* obtained from the statistical results of the plane channel flow with *hybrid version B* is depicted in Fig. 7 (right). From that figure it is clear that the ratio never passes below 0.3 (value at the position $y_2^* = 12$ or $y^+ \approx 7$) in the relevant RANS region and reaches 0.65 close to the interface ($y_2^* = 60$ or $y^+ \approx 30$). This result exhibits the importance of the resolved field in the RANS region and the persistence of the resolved scales. The significant level of the resolved field is plausible due to the position of the interface relatively close to the wall as well as the high resolution of the grid used in this particular simulation. The following questions are arising: How should $\nu^{\text{mod}}_{t,\text{RANS}}$ be readjusted? Should this adjustment be performed according to $(\overline{u'v'})_{\text{res}}$? If yes, how should the resolved Reynolds shear stress field be "introduced" in the RANS formulation?

Assuming that the second question can be answered positively, the remaining one is how to adjust the eddy viscosity. A natural choice to observe the importance of the resolved shear stress in the simulation is the ratio $(\overline{u'v'})_{\text{res}}/(\overline{u'v'})_{\text{tot}}$. A function providing this ratio is an interesting starting point and the adjustment of $\nu^{\text{mod}}_{t,\text{RANS}}$ then resembles to $\left[\nu^{\text{mod}}_{t,\text{RANS}} = \nu^{\text{mod,temp}}_{t,\text{RANS}} \cdot (1 - f)\right]$ with f representing the effect of $(\overline{u'v'})_{\text{res}}$. In order to verify these assumptions, an empirical function $f(y_2^*)$ mimicking the ratio $(\overline{u'v'})_{\text{res}}/(\overline{u'v'})_{\text{tot}}$ (Fig. 7, right)

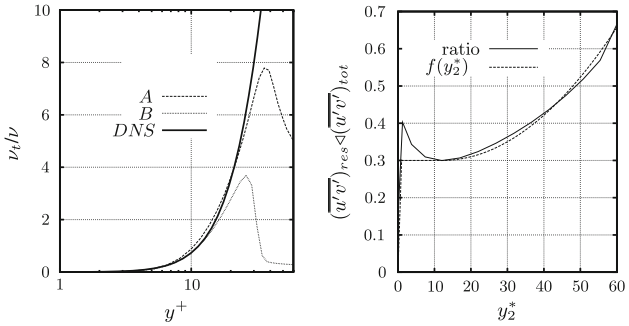

Fig. 7 Channel flow test case at $Re_\tau = 590$. $\nu_{t,\mathrm{RANS}}^{\mathrm{mod}}/\nu$ (*left*) for the *hybrid versions A* and *B* and the theoretical curve derived by DNS data. Ratio $(\overline{u'v'})_{\mathrm{res}}/(\overline{u'v'})_{\mathrm{tot}}$ for the *hybrid version B* and function $f(y_2^*)$ (*right*). LES–RANS interface at $y_2^* = 60$ ($y^+ \approx 30$) for *version B*

is formulated as a feasibility test before further developments are carried out. It reads

$$\begin{cases} f(y_2^*) = 0.3 \cdot y_2^* & \text{for } 0 \le y_2^* \le 1 \\ f(y_2^*) = 0.3 & \text{for } 1 < y_2^* \le 12 \\ f(y_2^*) = 0.3 + \left(1.55 \times 10^{-4}(y_2^* - 12)^2\right) & \text{for } 12 < y_2^* \le 60 \end{cases} \tag{16}$$

This function $f(y_2^*)$ compensating for the presence of $(\overline{u'v'})_{\mathrm{res}}$ in the formulation of $\nu_{t,\mathrm{RANS}}^{\mathrm{mod}}$ is used as follows. First $\nu_{t,\mathrm{RANS}}^{\mathrm{mod}}$ is calculated as previously mentioned in *hybrid version B* providing $\nu_{t,\mathrm{RANS}}^{\mathrm{mod,temp}}$. In a second step the function $f(y_2^*)$ is applied supplying the effective $\nu_{t,\mathrm{RANS}}^{\mathrm{mod}}$. An important remark is that the function $f(y_2^*)$ is not dynamically predicted within the simulation and is designed for *hybrid version B*. This is denoted *"Bf"*.

The results obtained by the implementation of this empirical function have been judged encouraging (Sect. 7.1.2) so that a new non-empirical function f was designed to replace the empirical formulation $f(y_2^*)$. This new function is dynamically predicted within the simulation and thus can be applied to each hybrid version. f is defined as follows

$$f = \frac{(u'v')_{\mathrm{res}}}{(u'v')_{\mathrm{res}} + (\overline{u'v'})_{\mathrm{mod}}} \quad \text{with } (u'v')_{\mathrm{res}} = (u - \overline{u}) \cdot (v - \overline{v})\,. \tag{17}$$

$\overline{(.)}$ has to be understood as the averaged value in time and homogeneous directions (if available). The use of $(\overline{u'v'})_{\mathrm{mod}}$ in f has been found to give better results than formulations without averaging especially by keeping an acceptable level of modeled eddy viscosity $\nu_{t,\mathrm{RANS}}^{\mathrm{mod}}$. The suffix "*fdyn*" is used in the appellation of an hybrid variant when the dynamic function is applied. As noticed for the interface type *B*, the method could be blamed for not being self-starting. However, in order to account for this feature the computations performed with the function f contains three phases before collecting statistics which are briefly mentioned. First, the simulation is computed without function f so that the flow develops. In a second phase, the averaging of $\overline{u'v'}_{\mathrm{mod}}$ found in (17) starts. After a short period ($\approx$ 2 flow-through times), f is applied for a few flow-through times ($\approx$ 5). Finally, the statistics are collected. Nevertheless, in order to improve the self-starting character of the simulations (namely to compute the whole simulation with f) the techniques mentioned in Sect. 2.3 can be consider.

A remark has to be added concerning this eddy-viscosity correction. Indeed, a similar idea of adjustment has already been performed by Templeton et al. [51]. However, they used a different formulation and it has been executed in the context of wall modeling for LES (not for an hybrid LES–RANS approach). Their technique relies on tabulated data of the wall-shear stress and the eddy-viscosity distribution obtained from averaged data of a resolved LES of channel flow at $Re_\tau = 395$, which makes it applicable to this flow case only, whereas the present approach (17) is more general.

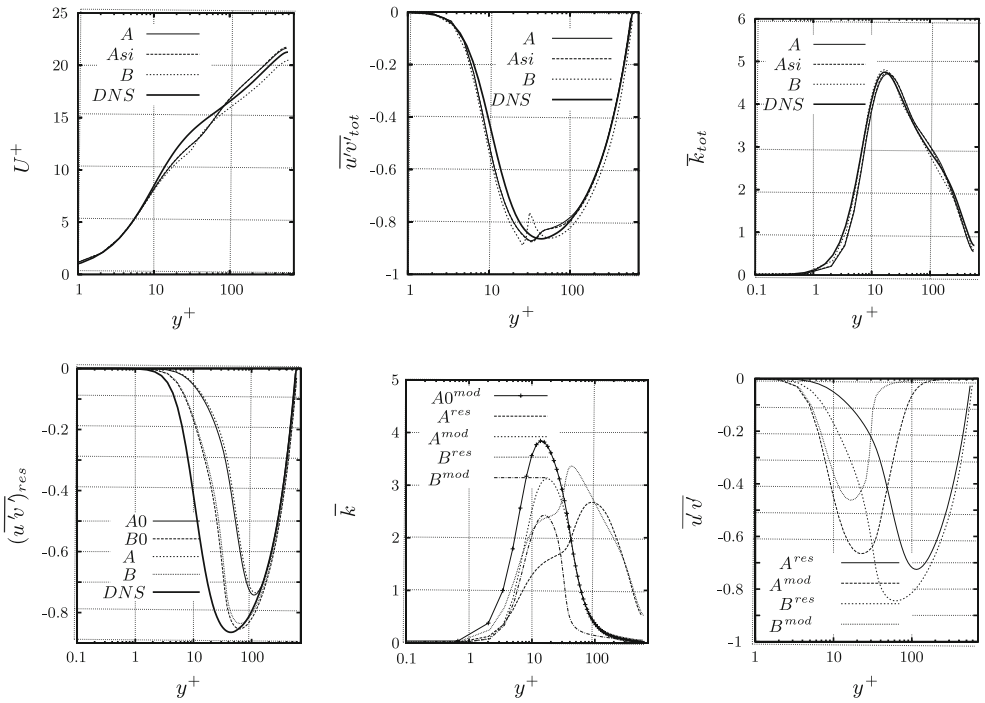

Fig. 8 Channel flow test case at $Re_\tau = 590$ on grid $\mathcal{F}$. Predictions of the mean streamwise velocity U^+ (*upper left*), the total Reynolds shear stress $\overline{u'v'}_{\text{tot}}$ (*upper center*) and the total turbulent kinetic energy $\overline{k}_{\text{tot}}$ (*upper right*) for the *hybrid versions A, Asi* and *B*. Resolved Reynolds shear stress $\overline{u'v'}_{\text{res}}$ (*lower left*). Distributions of the modeled ($A0^{\text{mod}}$, A^{mod} and B^{mod}) and resolved (A^{res} and B^{res}) turbulent kinetic energies for *hybrid versions A0, A* and *B* (*lower center*). Distributions of the modeled (A^{mod} and B^{mod}) and resolved (A^{res} and B^{res}) Reynolds shear stresses $\overline{u'v'}$ for the *hybrid versions A* and *B* (*lower right*). Values scaled by u_τ of each case, respectively. DNS data provided by Moser et al. [26]

7 Results

7.1 Channel flow at $Re_\tau = 590$

7.1.1 Versions A, Asi and B

The first modification carried out on the near-wall model (Sect. 6.1) as well as the interface criterion *Asi* are assessed on both grids $\mathcal{F}$ and $\mathcal{C}1$. Regarding the interface location, the sharp-interface *version Asi* switches at $y^+ \approx 45$ (since a precise value cannot be given owing to the range of positions, this is an approximation).

Concerning grid $\mathcal{F}$, which was also used in Sect. 5, only a marginal variation of the resolved field is visible as depicted in Fig. 8 (lower left). However, the total turbulent kinetic energy given by the DNS is now predicted accurately by each *hybrid version* (Fig. 8). The modeled and resolved contributions of the turbulent kinetic energy can also be seen in Fig. 8 (lower center). This as well as the equivalent graph for the Reynolds shear stress (Fig. 8, lower right) supply another evidence of the influence of the interface location, which was pointed out in Sect. 5. Comparing *hybrid versions A0* (RANS model with original set of constants by Rodi et al.) and *A* depicted in Fig. 8 (lower center), one can easily see that the adjustment of the RANS model leads to a reduction of the modeled turbulent kinetic energy. However, as previously mentioned, $\overline{k}_{\text{res}}$ is kept nearly unchanged. The u_τ value for *versions A* and *B* are equivalent (although slightly better) compared to *versions A0* and *B0*, respectively. The version *Asi* provides u_τ with a deviation of -2.26% with respect to the DNS value. The prediction of the mean streamwise velocity U^+ is also nearly unchanged (Fig. 8). Both *hybrid versions A* and *Asi* show familiar deviations from the DNS at the interface location and are almost not distinguishable over the entire y^+ range. One noteworthy point, which was previously not noticed because of missing modeled data, is a kink observed around the interface in the predictions of the total Reynolds shear stress $\overline{u'v'}_{\text{tot}}$ (Fig. 8, upper center). This behavior can be explained by scrutinizing Fig. 8 (lower right). In both versions *versions A* and *B* the modeled contribution $\overline{u'v'}_{\text{mod}}$ experiences a strong drop at the interface, which is not compensated

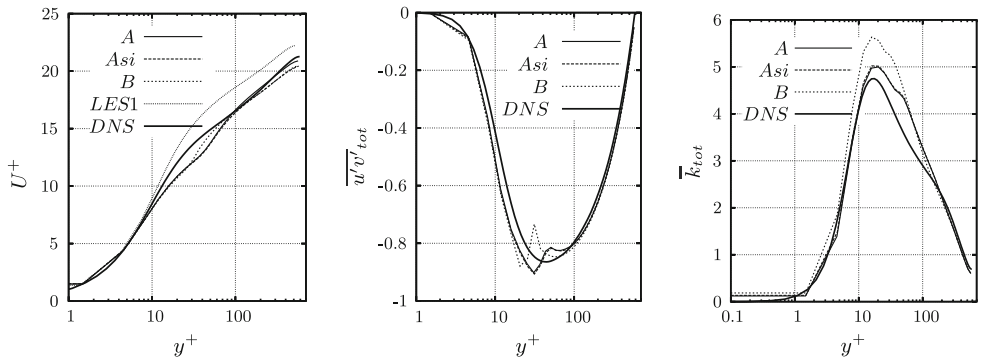

Fig. 9 Channel flow test case at $Re_\tau = 590$, results of *hybrid versions A, Asi* and *B* on grid $\mathcal{C}1$. Predictions of the mean streamwise velocity U^+ (*left*), the total Reynolds shear stress $\overline{u'v'}_{\text{tot}}$ (*center*) and the total turbulent kinetic energy $\overline{k}_{\text{tot}}$ (*right*). DNS result of Moser et al. [26]

by the resolved scales. This kink is another impact of the interface similar to the inflection point in the U^+ velocity profile mentioned in Sect. 5. It can be observed that this kink is not as pronounced for *version A*. The explanation is probably that the interface of *version A* is not as clear as in *version B*, providing a kind of unexpected "blending region". The drop of $\overline{u'v'}_{\text{res}}$ for the *variant A* being slightly weaker (weaker slope) than in *B* (Fig. 8, lower right) accredits this assumption. Moreover, a slight overprediction of $\overline{u'v'}_{\text{tot}}$ can be seen in the RANS region in both versions. Finally, the *hybrid versions A* and *Asi* exhibit equivalent results.

The results obtained on the coarser grid $\mathcal{C}1$ (Fig. 9) are not fundamentally different than the ones generated by grid $\mathcal{F}$. This satisfactory stability in the results with two different grid resolutions is not observed in the case of LES using the Smagorinsky model [40]. Indeed, the LES using the Smagorinsky model on grid $\mathcal{F}$, although not shown here, is in good agreement with the DNS, whereas on grid $\mathcal{C}1$ the mean streamwise velocity U^+ is strongly overestimated in the logarithmic region (Fig. 9, left). The moderately coarse resolution of grid $\mathcal{C}1$ appears to already be an obstacle for the LES using the Smagorinsky model. U^+ is reasonably predicted in each hybrid case. Nevertheless, the inflection point remains. Slight differences between the *versions A* and *Asi* are visible above $y^+ = 100$. This can be the consequence of the coarser grid spacing $\mathcal{C}1$, which can amplify hardly perceptible differences on grid $\mathcal{F}$ in this situation. However, the curves stay in good agreement with the DNS data [26]. u_τ is slightly better predicted ($+0.33$, $+2.09$ and $+1.78\%$ for *A, Asi* and *B*, respectively, compared with -1.96, -2.26 and $+3.22\%$ for *A, Asi* and *B* on grid $\mathcal{F}$). It is notable that both versions (*A* and *B*) on grid $\mathcal{C}1$ converge towards the reference solution, whereas their behavior in the logarithmic region on grid $\mathcal{F}$ is different (overprediction for *A* but underprediction for *B*). The kink in the prediction of $\overline{u'v'}_{\text{tot}}$ for the hybrid simulations is still observed (Fig. 9, center). The total turbulent kinetic energy is slightly overpredicted by the hybrid simulations (Fig. 9, right). The distributions of the modeled and resolved parts in comparison with grid $\mathcal{F}$ show that the resolved contribution is increased. Conversely, the modeled kinetic energy is similar from one grid to the other. This increased energy phenomenon has also been observed by Breuer [6] in the LES context when the grid is coarsened. Overall, the *hybrid versions A* and *Asi* present almost identical curves. The advantage of *Asi* is not obvious in the present situation. The influence of the RANS islands in the LES region on the results seems to be weak. This statement was also assumed by De Langhe et al. [12] who encountered a similar behavior in their hybrid LES–RANS approach. Moreover, Fig. 1 presents snapshots of the LES–RANS fields. This signifies that a RANS spot appearing at one time step may not be observed at the next one. Thus, this phenomenon is not thought to have a real impact on the statistical results.

7.1.2 Compensating functions $f(y_2^*)$ and f

The results presented are based on grids $\mathcal{F}$ and $\mathcal{C}1$. The dynamic function (17) designed to compensate the high level of resolved scales in the RANS region (Sect. 6.2) has been applied to the *hybrid versions A, Asi* and *B*. The empirical function (16) devoted to *variant B* is also presented. The results are depicted in Figs. 10, 11. It is obvious that the distribution of the mean velocity profile U^+ (Figs. 10, 11) is significantly improved by the application of the functions in the RANS region. Besides, both dynamic and empirical functions give similar results (Fig. 11, upper left). A slight deviation from the DNS data can still be observed around the interface. Nevertheless, the amplitude of the unphysical step is apparently reduced. The behavior of the model

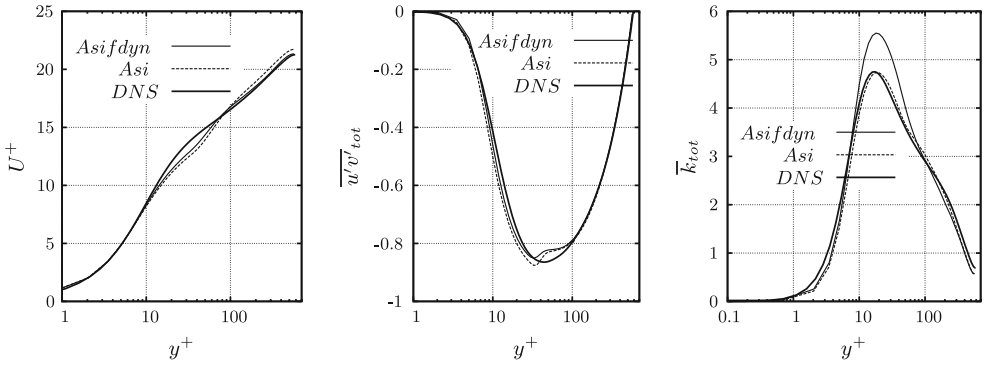

Fig. 10 Channel flow test case at $Re_\tau = 590$, results of *hybrid versions Asi* and *Asifdyn* on grid $\mathcal{F}$. Predictions of the mean streamwise velocity U^+ (*left*), the total Reynolds shear stress $\overline{u'v'}_{\text{tot}}$ (*center*) and the total turbulent kinetic energy $\overline{k}_{\text{tot}}$ (*right*). DNS result of Moser et al. [26]

at the interface is presently studied in order to propose a solution to resolve this remaining discrepancy. The prediction of u_τ is also enhanced. This statement is obvious on grid $\mathcal{F}$. Regarding the *versions A* and *Asi*, the deviations to DNS are -1.5 and -1.03% for *Afdyn* and *Asifdyn*, respectively, compared with -1.96 and -2.26 for *A* and *Asi*. For the *version B*, this is manifested by the following variations: $+0.26$ and $+1.2\%$ for *Bf* and *Bfdyn*, respectively, compared with $+3.22\%$ for *B*. On grid $\mathcal{C}1$, the *version Asifdyn* shows an improvement (from $+2.09\%$ for *Asi* to $+0.28\%$ for *Asifdyn*), whereas the remaining variants provide similar predictions. Regarding k, the reduction of the modeled part $\overline{k}_{\text{mod}}$ in the RANS region is apparent (Fig. 11, lower center). Nevertheless, this decrease does not balance the increase of the resolved turbulent kinetic energy $\overline{k}_{\text{res}}$ (Fig. 11, lower left), which results in the overprediction of the total contribution $\overline{k}_{\text{tot}}$ (Figs. 10, 11). Another interesting remark concerns the $(\overline{u'v'})_{\text{tot}}$ kink (Figs. 10, 11). Although it does not completely disappear, the magnitude is significantly reduced owing to the modified formulation of the eddy viscosity.

The functions are presently used to adjust $\nu_{t,\text{RANS}}^{\text{mod}}$ according to the proportion of $(\overline{u'v'})_{\text{res}}$ in the RANS region, which leads to its reduction (Fig. 11, lower right). However, the purpose is not to reach an LES-like eddy-viscosity level. A first evidence is given by comparing $\overline{k}_{\text{mod}}$ computed by the hybrid simulations with an LES using the one-equation model of Schumann [37] (LES2, Table 2). The former are significantly higher (Fig. 11, lower center). In order to further verify this point, the ratio of the eddy viscosity to the molecular viscosity is checked. The maximal averaged values of the ratio $\nu_{t,\text{RANS}}^{\text{mod}}/\nu$ on grid $\mathcal{F}$ are 3.7, 1.3, 1.25 and 0.2 for the *hybrid versions B*, *Bf*, *Bfdyn* and LES3, respectively. Thus, although the functions drive the hybrid LES–RANS method regarding the eddy-viscosity values towards an LES level, the $\nu_{t,\text{RANS}}^{\text{mod}}$ amplitude is still much larger than in LES (Fig. 11, lower right). Moreover, these results concerns the *hybrid versions B*, which offers lower modeled contributions and $\nu_{t,\text{RANS}}^{\text{mod}}$ values than the *versions A* and *Asi*. Regarding *variant A*, the maximal averaged ratios $\nu_{t,\text{RANS}}^{\text{mod}}/\nu$ for grid $\mathcal{F}$ are 7.65 and 4.2 for *A* and *Afdyn*, respectively. Thus, as expected the $\nu_{t,\text{RANS}}^{\text{mod}}$ level is larger than for the *versions B* and much larger than in the LES case.

7.2 Channel flow at $Re_\tau = 2,003$

Since the final objectives of hybrid methods is to tackle high-Re flows, in this section the *hybrid variants A, Asi* and *B* are assessed on the same channel flow configuration but at higher Reynolds number, i.e., $Re_\tau = 2,003$.

The general behavior of the method found for $Re_\tau = 590$ remains for the computations at $Re_\tau = 2,003$ (Figs. 12, 13). The methods *A* and *Asi* supply basically the same results. This strengthens the assumption that the switching back to RANS in LES mode is not as critical for the results. Besides, the number of RANS spots in LES is significantly reduced compared with the channel flow at $Re_\tau = 590$. This follows from the increased level of turbulent kinetic energy in the channel flow at $Re_\tau = 2,003$ compared to $Re_\tau = 590$ (Fig. 12, lower left). Subsequently, the modeled contribution $\overline{k}_{\text{mod}}$ in the hybrid approach also grows in the core region (comparison of $A^{\text{mod},590}$ and $A^{\text{mod},2,003}$ in Fig. 12, lower center). Thus, $\overline{k}_{\text{mod}}$ moves further away from the critical value k_{crit} defining the LES–RANS border (Sect. 2.3), which produces fewer islands (Fig. 12, lower right).

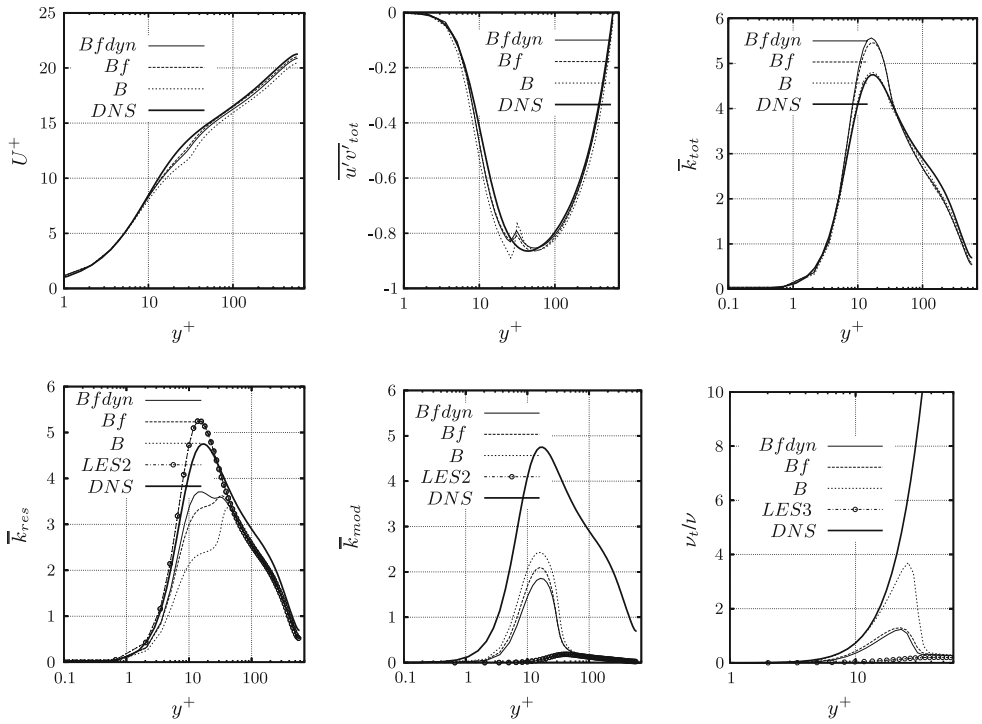

Fig. 11 Channel flow test case at $Re_\tau = 590$, results of the *hybrid versions B*, *Bf* and *Bfdyn* on grid $\mathcal{F}$. Mean streamwise velocity U^+ (*upper left*). Total Reynolds shear stress $\overline{u'v'}_{\text{tot}}$ (*upper center*). Total turbulent kinetic energy $\overline{k}_{\text{tot}}$ (*upper right*). Resolved turbulent kinetic energy $\overline{k}_{\text{res}}$ (*lower left*). Modeled turbulent kinetic energy $\overline{k}_{\text{mod}}$ (*lower center*). Normalized averaged modeled turbulent viscosity $\nu_{t,\text{RANS}}^{\text{mod}}/\nu$ (*lower right*). LES–RANS interface at $y^+ \approx 30$. DNS data provided by Moser et al. [26]

Concerning the normalized mean streamwise velocity U^+ the RANS region is similarly underestimated (Figs. 12, 13). The *version B* suffers from the "DES buffer layer" earlier than the two other variants as its interface is located closer to the wall as a consequence of the switching criterion. *Versions A* and *Asi* cannot be really distinguished. It is obvious that the shift-up produced at the interface is more pronounced for *B* than for the *variants A* and *Asi*. For grid $\mathcal{F}$, except a slight underestimation for the *hybrids A* and *Asi* the slope of the logarithmic layer is satisfactorily reproduced. The coarse resolution ($\mathcal{C}2$) seems to amplify the "DES buffer layer". The fine resolution of grid $\mathcal{F}$ might yield the LES recovery in the vicinity of the interface. For comparison an LES prediction performed on grid $\mathcal{C}2$ with the Smagorinsky model (LES4, Table 2) is added in Fig. 13. As visible it does not perform well. U^+ is underestimated until $y^+ \approx 30$. Regarding the logarithmic region, LES4 provides, as already noticed at $Re_\tau = 590$, a velocity profile which is less accurate than that of the hybrid method. Comparing the results of both Reynolds numbers the main difference is remarked in the distribution of $\overline{k}_{\text{tot}}$ (Figs. 12, 13). Here, a strong overestimation characterizes the hybrid method. By comparing the predictions of $\overline{k}_{\text{mod}}$ at $Re_\tau = 590$ and 2,003 on grid $\mathcal{F}$ (same grid for both Re_τ), no variation is noticed near the wall (Fig. 12, lower center). However, the situation differs for $\overline{k}_{\text{res}}$. Although Fig. 12 (lower left) displays a growth of $\overline{k}_{\text{tot}}$ between the DNS at $Re_\tau = 590$ (DNS1) and 2,003 (DNS2), $\overline{k}_{\text{res}}$ undergoes an important intensity increase, which is much larger than the one observed for DNS (Fig. 12, lower center). This can be explained by the tendency of LES to produce more turbulent kinetic energy under coarse grid resolution (Table 1).

7.3 Summary of channel flow results

Over the range of simulations performed the results are satisfactory. Regarding the LES–RANS interface, the tests carried out on the plane channel flow lead to various comments. The comparison between *variants A* and *Asi* tend to show that the RANS spots located in the LES core-region are not critical concerning the statistical results. The definition of the criterion y^* is based on the instantaneous value of k_{mod}, which signifies that a RANS island perceptible at one time step may not show up at the following one. Thus, in a statistical point of view the influence of these RANS spots appears to be weak. Besides, the phenomenon gets weaker as the

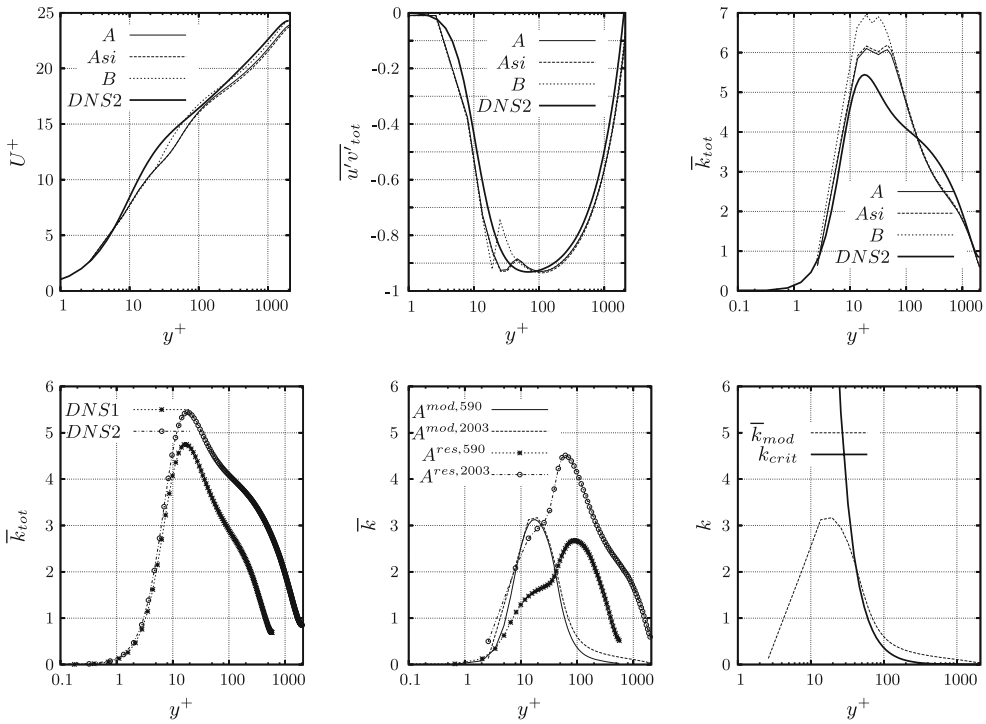

Fig. 12 Channel flow test case at $Re_\tau = 2,003$, results of *hybrid versions A, Asi* and *B* on grid $\mathcal{F}$. Predictions of the mean streamwise velocity U^+ (*upper left*), the total Reynolds shear stress $\overline{u'v'}_{\text{tot}}$ (*upper center*) and the total turbulent kinetic energy $\overline{k}_{\text{tot}}$ (*upper right*). DNS2: DNS at $Re_\tau = 2,003$ of Hoyas and Jiménez [18]. Comparison of the total turbulent kinetic energy between the DNS at $Re_\tau = 590$ (*DNS1*) and the DNS at $Re_\tau = 2,003$ (*DNS2*) (*lower left*). Distributions of the modeled and resolved turbulent kinetic energy at $Re_\tau = 590$ ($A^{\text{mod},590}$ and $A^{res,590}$, respectively) and the modeled and resolved turbulent kinetic energy at $Re_\tau = 2,003$ ($A^{\text{mod},2,003}$ and $A^{res,2,003}$, respectively) for *hybrid version A* (*lower center*). Behavior of $\overline{k}_{\text{mod}}$ in comparison with k_{crit} for *hybrid version A* (*lower right*)

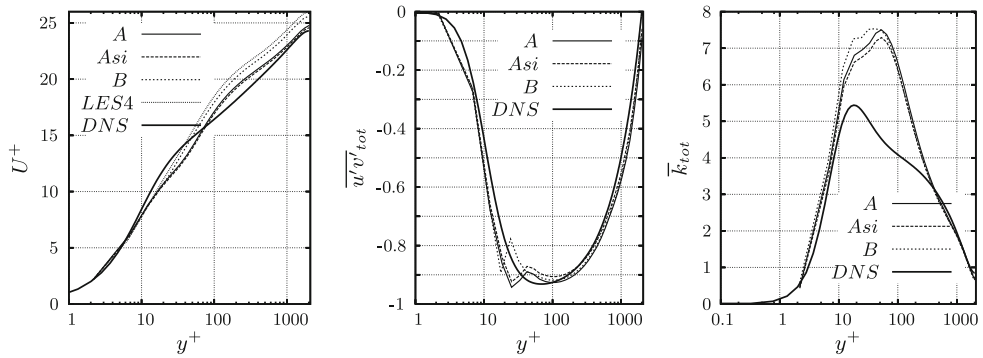

Fig. 13 Channel flow test case at $Re_\tau = 2,003$, results of *hybrid versions A, Asi* and *B* on grid $\mathcal{C}2$. Predictions of the mean streamwise velocity U^+ (*left*), the total Reynolds shear stress $\overline{u'v'}_{\text{tot}}$ (*center*) and the total turbulent kinetic energy $\overline{k}_{\text{tot}}$ (*right*). DNS result of Hoyas and Jiménez [18]

Reynolds number increases. Hence, since the *hybrid variant A* represents a cheaper formulation than *Asi*, the former is preferred.

The so-called "DES buffer layer" is present in each hybrid case as generally seen in various hybrid LES–RANS approaches proposed in the literature (Sect. 1). However, the intensity of the phenomenon varies according to the switching criterion or the grid resolution applied. The compensating function also has an enhancing effect on this issue. Indeed, in addition to provide closer results with respect to the DNS, the empirical and dynamic functions reduce the shift-up in the prediction of U^+ as well as for other values such as $\overline{u'v'}_{\text{tot}}$.

The *hybrid version A* gives a clear advantage over *B* in terms of RANS domain extension and ratios between the modeled and resolved contribution levels (higher level of modeled scales for *variant A*). Although the predictions of U^+ do not exhibit any clear advantage to *variant A* or *B*, conversely the former is inclined to predict $\overline{u'v'}_{\text{tot}}$ in a better agreement (especially a smoother curve at the LES–RANS interface). Thus, the preference goes to the interface type *A*. As seen in Sect. 7.4, the periodic hill flow test case will also yield a slight preference to *variant A*.

Another point is the constancy in the behavior and results of the hybrid LES–RANS approach observed over the various assessments carried out, i.e., different Reynolds numbers as well as fine and coarse grid resolutions. This stability is not noticed for LES, which for coarse resolution is not able to reproduce the logarithmic layer correctly.

Moreover, the hybrid version *A* has been assessed on the channel flow test case at $Re_\tau = 20,000$. The grid used is based on grid $\mathcal{F}$ excepting the wall-normal stretching factor which is increased to 1.115 in order to keep $y^+_{\text{1st pt}} \lesssim 2$. The resolution reaches values such as $\Delta x^+ = O(980)$ and $\Delta z^+ = O(490)$, which is far beyond the wall-resolved LES requirements whereas in the wall-normal direction the first grid point is located at $y^+_{\text{1st pt}} \approx 1$. As the prediction of U^+ taking the law of the wall as reference remains equivalent in terms of behavior to the comportment observed for $Re_\tau = 590$ and 2,003, this has not been included here. The near-wall region is slightly underestimated whereas the logarithmic region is somewhat overestimated behind the "DES buffer layer" although its slope is recovered.

7.4 Periodic hill flow simulation at $Re_b = 10,595$

The second, reasonably complex test case is the flow over periodic hills (Sect. 4.2). In addition to the hybrid approaches *A, Asi* and *B*, a DES applying the SA model and an LES using the Smagorinsky model have been performed (Table 3).

7.4.1 Extension of the LES and RANS zones

The RANS and LES domains are shown in Fig. 14 whereas Table 4 presents the repartition of the RANS CV layers in the main regions. It has to be recalled that Fig. 14 presents snapshots of the domains. Besides, the time step at which the figures are extracted do not correspond one to each other. For the *hybrid version B*, the interface position occurs at a distance of 5–10 RANS cells from the wall (depending on the streamwise location). A large portion of the recirculation region ($x/h \approx 0.6$–3.5) contains ten RANS cells normal to the wall, whereas the hill crest, where the separation occurs, is covered by five cell layers. Concerning the reattachment zone ($x/h \approx 5$) seven CV layers are found in the RANS mode. For the *hybrid version A* the interface at the lower wall is located above 6–16 RANS cells with a similar RANS cell distribution as the *version B* over the main zones of concern (6–7 CVs around the separation point, 8–16 CVs in the recirculation region and 9–10 CVs around the reattachment location). It is of interest to note that for the hill flow test case the problem of a frayed LES–RANS interface (with RANS islands in the LES core region) encountered in the channel flow case nearly vanished. Solely on the upper wall and at a few locations on lower one the problem still persists. The features and the intensity of the distribution of the modeled turbulent kinetic energy at the lower wall for *variant A* are such that it sharply crosses the curve k_{crit} (Sect. 2.3) characterizing the LES–RANS interface (Fig. 15). The *hybrid version Asi* switches to LES at a wall-normal distance according to 6–18 CVs.

Besides, it is interesting that three different interface layouts are obtained. Although *hybrid version A* is characterized by the RANS islands, the *variant Asi* is RANS-island free. However, the interface of the last is rough (significant irregularities on the upper wall). *Version B* is RANS-island free and presents a smooth interface.

It is noteworthy to mention that the method minimizes automatically the number of RANS cells in the region of separation as a consequence of the high turbulent intensity near the wall in this region (Fig. 14, lower right). This statement is clearly visible in Fig. 14 and especially for the *hybrid versions A* and *B*. Regarding *Asi*, a local minimum of the RANS domain is observed at $x/h \approx 0.3$. A verification confirms that at this time step the beginning of the separated shear layer is pointed around this value. Here it is worth to report that the instantaneous separation point occurs on a streamwise location range of $x/h \approx -0.1$ to 0.7 according to Fröhlich et al. [14]. This can explain some differences noticed in Fig. 14 (e.g., the local minimum of the RANS region in the separation region does not correspond with the averaged value of the separation point given in Table 4). The region around the separation is characterized by large velocity gradients, which result

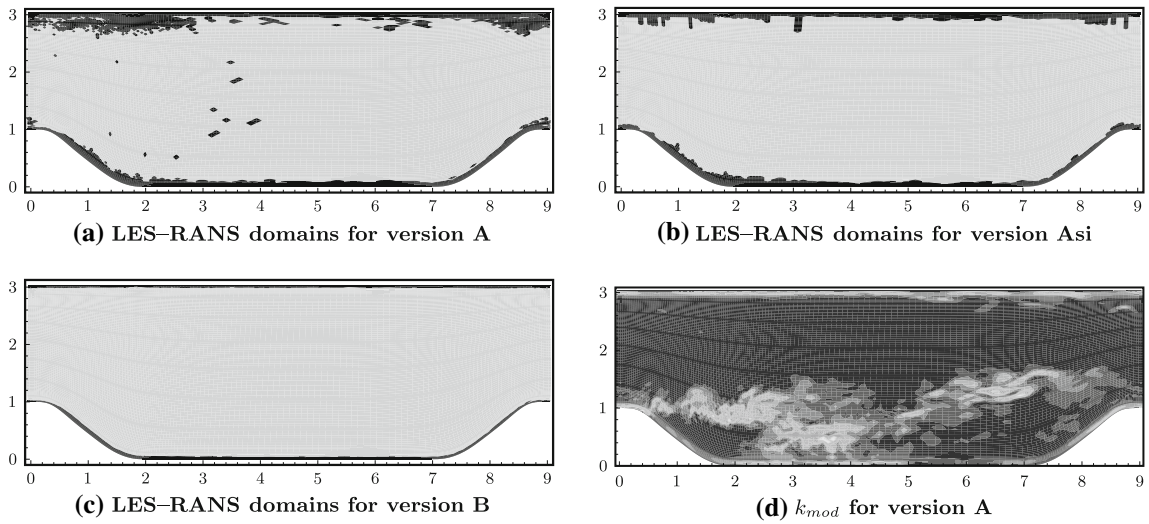

Fig. 14 Periodic hill flow at $Re_b = 10,595$. LES–RANS domain layout for *hybrid versions A* (*upper left*), *Asi* (upper right) and *B* (*lower left*). RANS domain *black zone*. LES domain *grey zone*. Distribution of the modeled turbulent kinetic energy k_{mod} for the *hybrid version A* (*lower right*). *Dark region* low k_{mod} intensity. *Bright region* high k_{mod} intensity

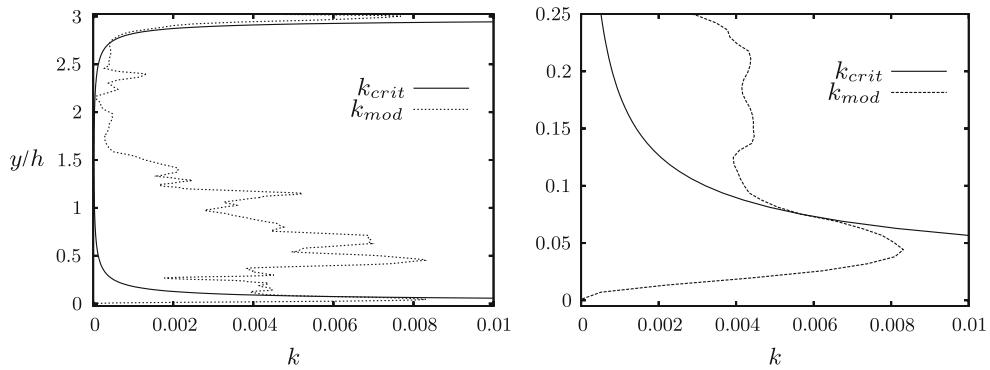

Fig. 15 Periodic hill flow at $Re_b = 10,595$. Interface behavior of the *hybrid version A*. Modeled turbulent kinetic energy k_{mod} at position $x/h = 4$ compared with k_{crit} representing the LES–RANS border. *Left plot* complete domain. *Right plot* zoom of the lower wall

Table 4 Periodic hill flow at $Re_b = 10,595$

Case	Separation		Recirculation	Reattachment	
	loc.	RANS	RANS	loc.	RANS
WR-LES	0.190	–	–	4.694	–
LES	0.201	–	–	4.547	–
DES	0.173	8	7–8	5.197	9
A	0.254	6–7	8–16	4.751	9–10
Asi	0.255	6–7	11–18	4.910	8–12
B	0.269	5	7–10	5.156	7

Separation and reattachment locations and number of RANS cells at the lower wall for the separation, core of recirculation ($x/h \approx 0.6$–3.5) and reattachment regions
loc location, *RANS* number of RANS cell layers

in an increased production term $\mathcal{P}$ in (1) and subsequently in the rise of the modeled turbulent kinetic energy around the separation location. Since the switching criterion is based on k_{mod}, it recognizes this phenomenon and echoes it through a thinner RANS region around the separation. This signifies that the interface condition y^* is able to locate the instantaneous separation point and that the local minimum of the RANS region moves according to this point. Thus, spatially the beginning of the separated shear layer is computed with a minimum of RANS modeling, which yields the simulation to compute almost the entire shear layer in LES mode.

Within the range $x/h \approx 0.6$–2 (Fig. 14, lower right), where the turbulent kinetic energy is low near the wall in comparison with the separation region, the RANS domain spreads. However, after $x/h \approx 2$–2.5, the intensity of k_{mod} increases near the wall. Here again, the method adapts itself to the turbulent flow features by progressively reducing the RANS region. Consequently, the reattachment region is computed with fewer RANS cells than in the range $x/h \approx 0.6$–2. Hence, the hill flow test case gives the first evidence that the present switching method based on k is, in this configuration, able to give priority either to LES or RANS by automatically detecting the zones of high or low turbulent intensity level, respectively.

7.4.2 Evaluation of the velocity profiles and the separation/reattachment points

The hill flow results of the different variants of the hybrid model are plotted together with DES results and the highly resolved LES data [7,9] denoted WR-LES. The mean velocity normalized with the bulk velocity U/U_b is plotted at the positions $x/h = 0.5$–8 (Fig. 16). The streamwise locations $x/h = 0.5$, 2 and 6 represent the beginning and the center of the recirculation region and the post-reattachment region, respectively. The mean velocity U is overall well reproduced by the new models at each streamwise position (Fig. 16, upper).

Since the recirculation region as well as the separated shear layer are the most important characteristics of the present flow, the analysis of U/U_b is focused on these zones (Fig. 16, lower). In the region prior to $x/h \approx 2$, the *variant B* provides, despite a somewhat delayed separation (Table 4), a slightly better agreement for the negative velocity part near the wall at positions $x/h = 0.5$ and 1 even if a weak underestimation is visible. The shear layer at these positions is in good agreement with the WR-LES solution for each hybrid version.

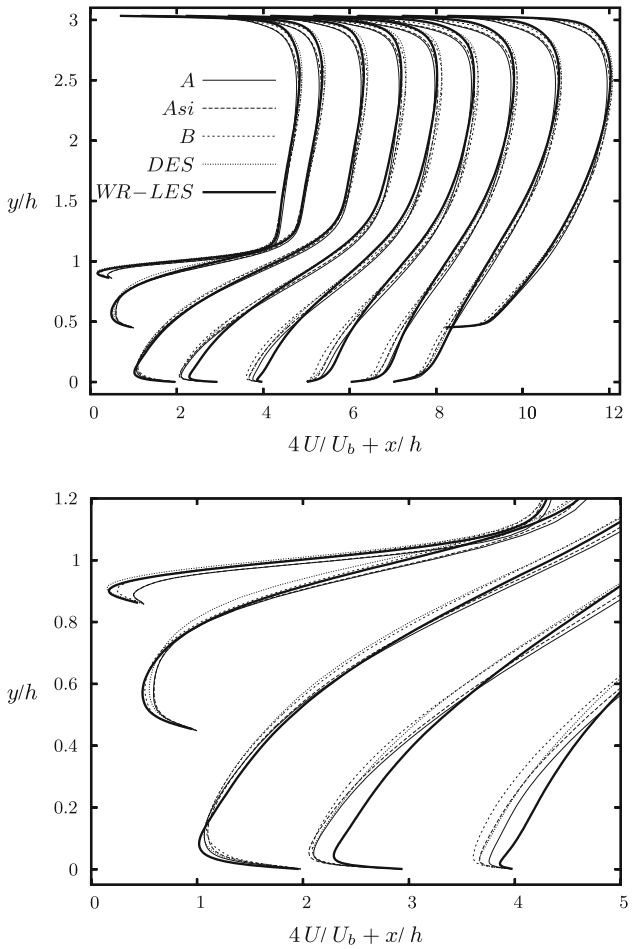

Fig. 16 Periodic hill flow at $Re_b = 10,595$. Mean velocity U/U_b. Comparison of the three *hybrid versions A*, *Asi* and *B* with DES and the wall-resolved LES prediction [7,9]. *Upper plot* complete domain. *Lower plot* zoom of the recirculation region. The same legend is used for both plots

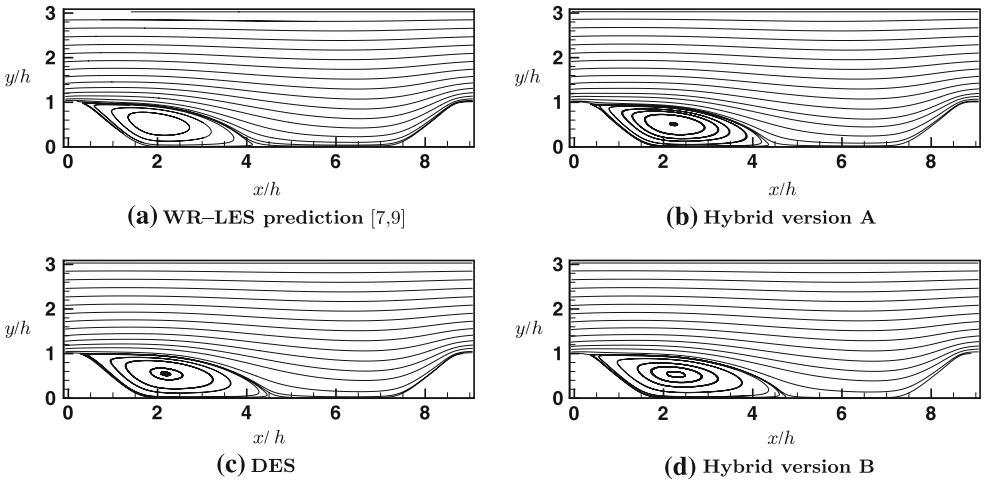

Fig. 17 Periodic hill flow at $Re_b = 10,595$. Streamlines of the averaged flow. Comparison of *hybrid versions A* and *B*, DES and the WR-LES prediction

At $x/h = 2$ the shear layer is still well predicted. The SGS model does not suffer from the RANS treatment applied at the wall. In the near-wall region, each hybrid version predicts similar peaks (slightly underestimated but close to the WR-LES curve) although *version A* is now closer to the highly resolved LES prediction than the other variants. At $x/h = 3$, the hybrid approach overestimates the negative peak in a similar manner for each variant. Between $x/h = 3.5$ and 4.5 the deviations get larger among the versions. *Variant A* supplies the best predictions followed by *Asi* and finally *B*. This statement remains valid in the post-reattachment region ($x/h = 6$). The DES exhibits similarly good results except in the near-wall region around the reattachment ($x/h = 4$–6) where an overprediction is observed in the pre-reattachment region but an underprediction in the post-reattachment zone. One remark is made on the fact that no manifestation of the interface presence is visible. In other words, a discrepancy such as the "DES buffer layer" observed for the channel flow is not perceptible here.

The separation/reattachment location study shows that the LES based on the Smagorinsky model predicts the best separation point with respect to the WR-LES prediction (Table 4). Whereas the DES underpredicts the separation location but stays in close agreement with WR-LES, the hybrid simulations somewhat delay this point. *Hybrid version A* gives slightly better results than *version B*. However, the variation is not large.

All hybrid and DES simulations show a delayed reattachment compared to WR-LES (Table 4). The *hybrid version B* is in closer agreement with the WR-LES data than the DES result. That also holds for the *hybrid Asi* which slightly overpredicts the reattachment point with respect to the WR-LES value. More interesting is that the *hybrid version A* shows the most accurate prediction, better than all other hybrids, the DES, and even the LES. In comparison with LES and DES, which show deviations of -3.1 and $+10.7\%$, respectively, *version A* leads to a deviation of $+1.2\%$ only. Figure 17 shows plots of the averaged streamlines for the *hybrid versions A* and *B*, the DES and the WR-LES solution. Both hybrid and DES techniques, for which the center of the recirculation zone is predicted similarly, exhibit slightly larger recirculation regions with respect to WR-LES. Moreover, in comparison with the WR-LES data, the location of the recirculation center is slightly shifted downstream. However, these three simulations still offer satisfactory results.

7.4.3 Evaluation of the Reynolds stress profiles

In general, the Reynolds stresses are well predicted by all hybrid variants (Fig. 18, left). The profiles are overall recovered with respect to WR-LES, especially for $\overline{u'u'}_{\text{tot}}$ and $\overline{u'v'}_{\text{tot}}$. Regarding $\overline{v'v'}_{\text{tot}}$, the apparition of peaks in the vicinity of the lower and upper walls not present in the WR-LES is noticed. The modeled contribution provided by the linear near-wall eddy-viscosity RANS model is responsible for this fact which is a well-known deficit of such models. Regarding the intensities, only slight under- or overestimations are observed in the predictions of $\overline{u'u'}_{\text{tot}}$ and $\overline{u'v'}_{\text{tot}}$. The underestimation is more pronounced for $\overline{v'v'}_{\text{tot}}$ but still reasonable. However, at the position $x/h = 0.5$ the *versions A* and *Asi* show discrepancies (underestimation) in the prediction of the peaks located in the vicinity of the lower wall for $\overline{v'v'}_{\text{tot}}$ and $\overline{u'v'}_{\text{tot}}$, which are not observed

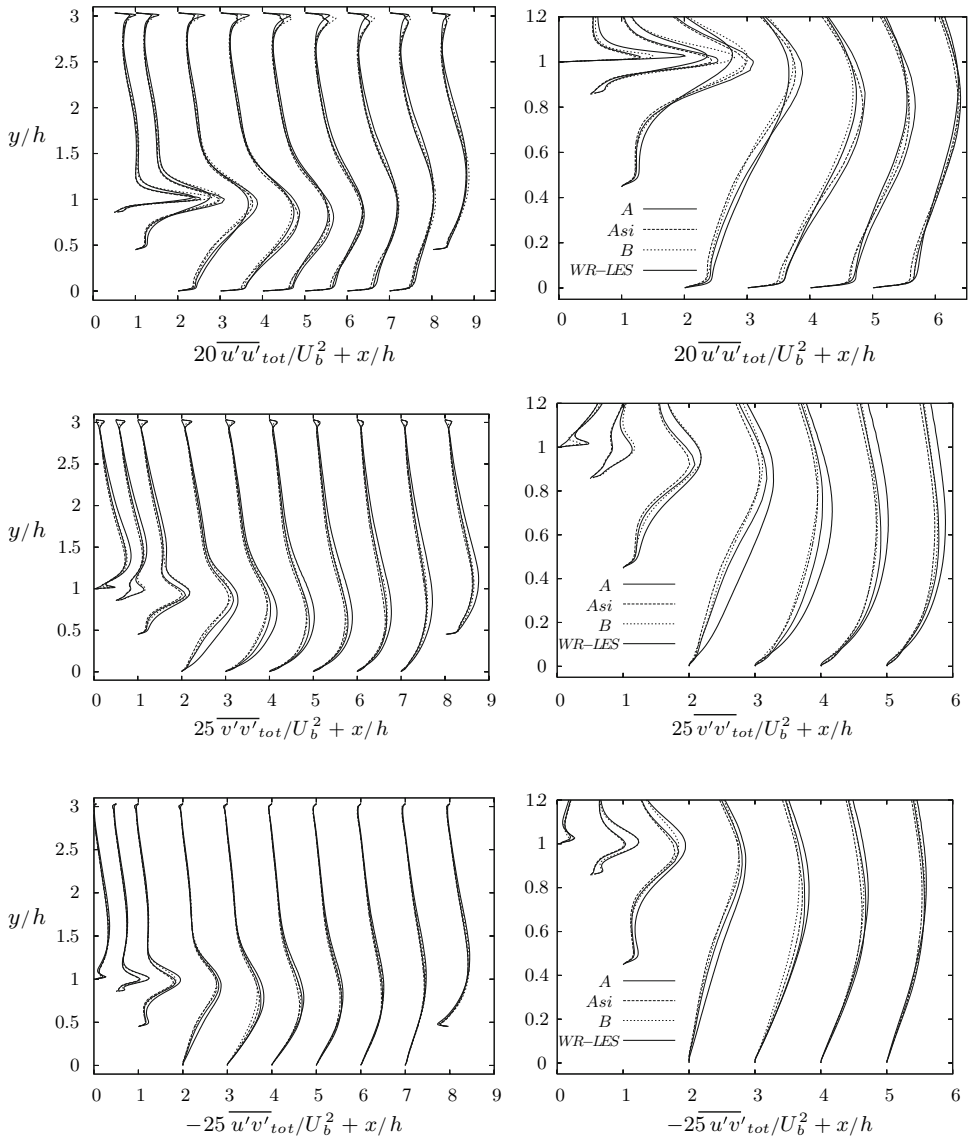

Fig. 18 Periodic hill flow at $Re_b = 10,595$. Total normal Reynolds stresses $\overline{u'u'}_{\text{tot}}$ (*upper*) and $\overline{v'v'}_{\text{tot}}$ (*middle*). Total Reynolds shear stress $\overline{u'v'}_{\text{tot}}$ (*lower*). *Left plots* complete domain. *Right plots* zoom of the recirculation region. The same legend is used for the plots on the left and right sides. For the sake of visibility the profile of $\overline{u'u'}_{\text{tot}}$ at position $x/h = 0.05$ is not plotted on the left-hand figure

in *version B*. The modeled stresses are similar in both simulations *A* and *B*, thus these underestimations mainly result from a lack of resolved scales in this region for the variants *A* and *Asi* compared with *version B* for which good agreement is obtained.

The analysis is now refined on the pre-separation region (Fig. 18, right). The best predictions of $\overline{u'u'}_{\text{tot}}$ among the hybrid versions are given by the *variant B*, especially for the main peak located at the lower wall. The *variants A* and *Asi* tend to underestimate this Reynolds stress. An equivalent remark is done for $\overline{v'v'}_{\text{tot}}$. Here, the discrepancy in the prediction of $\overline{v'v'}_{\text{tot}}$ for the *version B* mentioned above (peaks at the lower wall) is also smaller than for the *variants A* and *Asi*. In the range $x/h = 0.05$–0.3, the *variant B* again shows a better performance for $\overline{u'v'}_{\text{tot}}$. The local maximum located at $y/h \approx 1.5$ is best reproduced by *B*. Concerning the peak found at the lower wall, *version B* gives the best predictions for $x/h = 0.05$ and $x/h = 0.3$. Nevertheless, *A* and *Asi* show more agreement with WR-LES at $x/h = 0.1$ and 0.2 (not shown here).

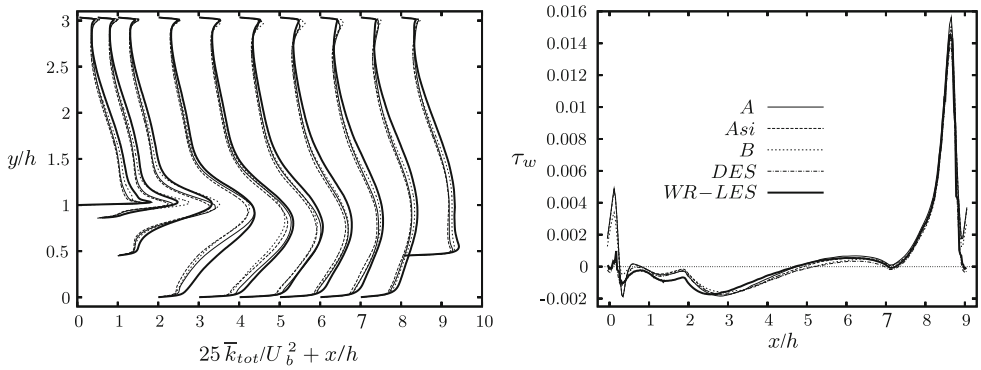

Fig. 19 Periodic hill flow at $Re_b = 10,595$. Total turbulent kinetic energy $\overline{k}_{\text{tot}}$ (*left*) of the *hybrid versions A*, *Asi* and *B* and the WR-LES prediction [7,9]. Wall shear stress τ_w at the lower wall (*right*) of the *hybrid versions A*, *Asi* and *B*, the DES and the WR-LES prediction. The same legend is used for both plots

The study is now focused on the post-separation and reattachment regions (Fig. 18, right). First, the normal Reynolds stress $\overline{u'u'}_{\text{tot}}$ is considered. Whereas the *version B* is generally superior to the others (mainly by the constancy of its predictions), near the lower wall in the recirculation region the *version A* shows better results. The *version B* tend to underpredict $\overline{u'u'}_{\text{tot}}$ whereas *version A* is closer to the WR-LES solution. This is clearly visible for the streamwise positions $x/h = 3$ to 4.5. The resolved contribution does not exhibit large variations among the variants in the near-wall region. By studying the modeled contribution $\overline{u'u'}_{\text{mod}}$, one can observe that the peak value near the wall supplied by the *versions A* and *Asi* is almost twice as large as for *B*. This lack of modeled scales originates from the LES–RANS interface location. Indeed, the *version A* offers a thicker RANS region, which leads to a higher value of the eddy viscosity near the lower wall. Thus, $\overline{u'u'}_{\text{mod}}$ is larger for *A* than for *B*. The latter seems to switch from RANS to LES at a critical position (high gradient). The RANS region does not spread enough to capture the entire near-wall peak. Here, the resolved field does not compensate the discrepancy as it starts vanishing in the RANS mode towards the wall. Conversely, the larger RANS extensions of *A* and *Asi* prevent this phenomenon as the near-wall peak is entirely taken into account by the RANS model. The maximal value of $\overline{u'u'}_{\text{tot}}$ located around $y/h = 1$ is also larger for *A* than for *B* due to a higher $\overline{u'u'}_{\text{res}}$ intensity. A similar behavior is detected for $\overline{v'v'}_{\text{tot}}$. However, in the range $x/h = 2$–5, version *A* gives the best predictions on the entire y/h range. For $\overline{u'v'}$, *B* provides the best predictions outside the recirculation region. However, in this special zone the *variant A* gives for the whole wall-normal range the closest results with respect to WR-LES. The same comments as for $\overline{u'v'}_{\text{tot}}$ are effective for the total turbulent kinetic energy $\overline{k}_{\text{tot}}$ (Fig. 19, left).

These observations can explain the differences in the prediction of the reattachment point. Indeed, this location is mainly governed by the turbulent fields in the recirculation region and the separated shear layer. In these regions the hybrid *version A* provides the best results. The higher turbulence intensity of the *variant A* leads to a shorter reattachment region.

7.4.4 Evaluation of the wall shear stress distribution

Concerning the wall shear stress distribution τ_w (Fig. 19, right), the hybrid simulations show at the hill crest larger deviations than the DES, which is in good agreement with the WR-LES. This behavior was also noticed in RANS simulations of the hill flow test case and is caused by a highly inaccurate prediction of the (modeled) Reynolds stresses. For the hybrid approach, the discrepancies found are caused by the same reason. Indeed, a strong peak (especially for *A* and *Asi* but also for *B*) appears in the prediction of $\overline{v'v'}_{\text{tot}}$ at $x/h = 0.05$ but is neither present in the WR-LES nor in the resolved contribution $\overline{v'v'}_{\text{res}}$ of the hybrid approach. This peak originates from the modeled field and thus from the RANS modeling leading to the τ_w deviations.

7.5 Summary of the hill flow results

In conclusion, all hybrid simulations give encouraging statistical results similar (or in some cases better) than DES. In a general point of view, one can conclude that the *hybrid version B* shows better predictions of higher-

order statistics than the *versions A* and *Asi*. However, if the study is localized on the governing flow features (separated shear layer and recirculation region) *hybrid version A* can be seen as superior in the prediction of the second-moment correlations. This statement is confirmed by the locations of separation and reattachment as well as the results concerning the mean streamwise velocity. For the latter, although the variations are not large over the entire domain, *hybrid version A* show the best performance in these crucial flow regions. This also holds for DES, which does not supply results as good as the *hybrid version A* with the exception of the separation region.

Here again, the comparison of the *hybrid versions A* and *Asi* sustains the idea that the RANS islands appearing in the LES core-region are not fundamentally prejudicial for the simulations. No indication of deterioration has been detected.

Regarding the interface criterion, it has been observed that the conditions y^* and y_2^* based on k are able to adapt itself to the flow conditions, what DES is not able to perform due to its interface condition involving a direct grid dependency.

Another interesting remark is the fact that no sign of any phenomenon such as the "DES buffer layer" is perceptible here.

Whereas the previous hybrid LES–RANS results shown for the channel flow test case were performed with the SGS model of Schumann (Sect. 2.1) in LES mode, the *hybrid LES–RANS versions A* and *B* were also assessed with the SGS model proposed by Sagaut [34] using $C_\mu = 0.062$ and $C_d = 1.0$ as constants. These tests (not shown here) were carried out in order to check the influence of the SGS model. The results showed a slight advantage of the model of Schumann.

Finally, the current study relies on a simple RANS model. Indeed, the substitution of the near-wall RANS model of Rodi et al. [33] by a more advanced formulation, such as an explicit algebraic Reynolds stress model (EARSM), may further improve the performance of the hybrid approach and avoids unphysical results, i.e., the strong $\overline{v'v'}_{\text{tot}}$ peak near the wall (or the underestimation of U^+ in the RANS region for the channel flow test case).

8 Conclusions

This study has focused on the hybrid LES–RANS technique. A new non-zonal hybrid LES–RANS approach which splits up the simulation into a near-wall RANS part and an outer LES part was suggested and tested. This technique is based on the association of a one-equation SGS model (LES zone) with the near-wall one-equation model proposed by Rodi et al. [33] in the RANS zone. The RANS model was adjusted to higher Reynolds numbers taking new DNS data into account. Furthermore, a second adjustment was suggested which takes into consideration that resolved scales are found in the near-wall RANS regions. These measures significantly improve the hybrid LES–RANS predictions. From a more general point of view, the investigations of this new approach reveal encouraging results for both, the plane channel flow and the periodic hill flow. These results were achieved with an interface formulation which avoids the usage of a reconstructed synthetic velocity field. That outcome is not astonishing for the separated hill flow case, but for the fully attached channel flow, which cannot rely on natural instabilities found in separated flows.

Regarding the test performed on the channel flow test case, the stability of the behavior observed between $Re_\tau = 590$ and 2,003 remains for the step from $Re_\tau = 2,003$ to 20,000. This positive comportment makes us optimistic in the capability of the method to be applicable to high Reynolds numbers, especially when the trend to underestimate the near-wall region is solved (compensating function, new RANS model such as EARSM, etc.).

Another topic was to study the newly suggested interface criterion based on the turbulent kinetic energy. Three alternatives have been proposed and their influence on the predictions checked. Among these three proposals, the version *A* based on the modeled turbulent kinetic energy has exhibited the most encouraging results. Moreover, it allows a larger expansion of the RANS region further away from the wall compared with the others what is advantageous from the practical point of view. Although a clear line of demarcation between RANS and LES region is occasionally missing, this particularity has not been found to deteriorate the predictions. Compared to the criterion defining a sharp interface *Asi* only marginal deviations are found for this version. An additional advantage of *A* (and *Asi*) is its self-starting character. Indeed, no time averaging (as well as averaging in homogeneous directions) is required in the formulation of y^*. However, the most interesting feature obtained with any of the three interface criteria is obviously that the method has shown abilities to adapt the LES–RANS interface location according to the flow conditions.

The current study relies on an interface treatment in its simplest form leading to phenomenon such as the "DES buffer layer" in the channel flow. However, as mentioned above *no sign of any phenomenon such as the DES buffer layer is perceptible* for the periodic hill flow. It is generally admitted that the "DES buffer layer" is the consequence of non-matching turbulence characteristics between the RANS and LES domains. The region where the different modeling approaches coexist is often related to "grey area". In this region, the LES mode has to reconstruct a suitable turbulence type for itself. In the channel flow test case the turbulence production is located in the vicinity of the wall and therefore in RANS mode. Thus, the LES cannot trust on other source of turbulence which could further stimulate the LES turbulence recovery. Conversely, the main source of turbulence for the hill flow test case is the separated shear layer, which in the present hybrid LES–RANS simulations is computed almost entirely in LES mode. The shear layer feeds a large portion of the flow with LES-type turbulence. Therefore, the LES–RANS interface region receives some turbulent fluctuations from the shear layer which as a consequence triggers the LES recovery. The problem is thus weakened compared with the channel flow test case. However, this does not signify that no interface treatment is necessary as the turbulence originating from the RANS region has still to be somehow adapted to LES requirements.

Here, the question of suitable grids for hybrid LES–RANS methods arises. Indeed, it is likely that a fine resolution in the grey area would help the LES recovery. However, this contradicts the philosophy of grid design for hybrid techniques.

The gain of CPU-time of the present method compared to LES has not been mentioned. Even if no detailed CPU-time comparison was carried out, it appears that the hybrid method provides better results on coarse grids where LES is already affected by the resolution. The constancy of the results obtained with the hybrid method after successive grid coarsening should also be noticed. In conclusion, the hybrid method is able to provide equivalent predictions as LES but on a much coarser resolution for which the gain of CPU-time is obvious.

Acknowledgements The project is financially supported by the *Deutsche Forschungsgemeinschaft* (BR 1847/8) and the *Centre National de la Recherche Scientifique* within the *French–German Programme* "LES for complex flows"(FOR 507). The computations were partially carried out at RRZE Erlangen and LRZ München. All kinds of support are gratefully acknowledged.

References

1. Baggett, J.S.: On the feasibility of merging LES with RANS in the near-wall region of attached turbulent flows. In: Annu. Res. Briefs-1998. Center Turbul. Res., Stanford University, California, pp. 267–277 (1998)
2. Batten, P., Goldberg, U., Chakravarthy, S.: LNS—an approach towards embedded LES. AIAA Paper 2002–0427 (2002)
3. Batten, P., Goldberg, U., Chakravarthy, S.: Interfacing statistical turbulence closures with large-eddy simulation. AIAA J. **42**(3), 485–492 (2004)
4. Breuer, M., Rodi, W.: Large-eddy simulation of complex turbulent flows of practical interest. In: Hirschel, E.H. (ed.) Flow Simulation with High-Performance Computers II, Notes on Numerical Fluid Mechanics, vol. **52**, pp. 258–274, Vieweg Verlag, Braunschweig (1996)
5. Breuer, M.: Large-eddy simulation of the sub-critical flow past a circular cylinder: numerical and modeling aspects. Int. J. Num. Methods Fluids **28**, 1281–1302 (1998)
6. Breuer, M.: Direkte Numerische Simulation und Large-eddy Simulation turbulenter Strömungen auf Hochleistungsrechnern. Habilitationsschrift, Univ. Erlangen–Nürnberg, Berichte aus der Strömungstechnik, ISBN: 3-8265-9958-6 (2002)
7. Breuer, M., Jaffrézic, B., Peller, N., Manhart, M., Fröhlich, J., Hinterberger, Ch., Rodi, W., Deng, G., Chikhaoui, O., Šarić, S., Jakirlić, S.: A comparative study of the turbulent flow over a periodic arrangement of smoothly contoured hills. In: Lamballais, E., Friedrich, R., Geurts, B.J., Métais, O. (eds.) Sixth International ERCOFTAC Workshop on DNS and LES: DLES-6, Poitiers, France, Sept. 12–14, 2005, ERCOFTAC Series, vol. 10, pp. 635–642, Direct and Large-eddy Simulation VI, ISBN-10 1-4020-4909-9, Springer, Heidelberg (2006)
8. Breuer, M., Jaffrézic, B., Šarić, S., Jakirlić, S., Deng, G., Chikhaoui, O., Fröhlich, J., von Terzi, D., Manhart, M., Peller, N.: Issues in hybrid LES–RANS and coarse grid LES of separated flows. EUROMECH Colloquium 469, Large-eddy Simulation of Complex Flows, TU Dresden, Germany, October 6–8, 2005
9. Breuer, M.: New reference data for the hill flow test case. personal communication, http://www.hy.bv.tum.de/DFG-CNRS/ (2005)
10. Davidson, L., Dahlström, S.: Hybrid LES–RANS: computation of the flow around a three-dimensional hill. In: Rodi, W., Mulas, M. (eds.) Engineering Turbulence Modeling and Experiments, vol. 6, pp. 319–328. Elsevier, Amsterdam (2005)
11. Davidson, L.: Hybrid LES–RANS: inlet boundary conditions. In: Skallerud, B., Andersson, H.I. (eds.) 3rd National Conference on Computational Mechanics—MekIT'05, Trondheim, Norway, 11–12 May 2005, pp. 7–22 (2005)
12. De Langhe, C., Merci, B., Lodefier, K., Dick, E.: Hybrid LES/RANS simulations of swirling confined turbulent jets. In: 4th International Symposium on Turbulence and Shear Flow Phenomena, USA, June 27–29, 2005, pp. 1147–1152 (2005)
13. Durbin, P.A.: Near-wall turbulence closure modeling without damping functions. Theoret. Comput. Fluid Dyn. **3**, 1–13 (1991)
14. Fröhlich, J., Mellen, C.P., Rodi, W., Temmerman, L., Leschziner, M.A.: Highly resolved large-eddy simulation of separated flow in a channel with streamwise periodic constrictions. J. Fluid Mech. **526**, 19–66 (2005)
15. Germano, M., Piomelli, U., Moin, P., Cabot, W.H.: A dynamic subgrid-scale eddy-viscosity model. Phys. Fluids A **3**, 1760–1765 (1991)

16. Germano, M.: From RANS to DNS: towards a bridging model. In: Voke, P.R., Sandham, N.D., Kleiser, L. (eds) Direct and Large-Eddy Simulation III, Proceedings of the Isaac Newton Institute Symposium/ERCOFTAC Workshop on Direct and Large-Eddy Simulation, Cambridge, 12–14 May 1999, ERCOFTAC Series, vol. 7, Kluwer, Dordrecht, 1999, pp. 225–236 (1999)
17. Hanjalić K., Hadžiabdić M., Temmerman L., Leschziner M.A.: Merging LES and RANS strategies: zonal or seamless coupling?. In: Friedrich et al. (eds.) Direct and Large-eddy Simulation V. Kluwer, Netherlands, pp. 451–464 (2004)
18. Hoyas, S., Jiménez, J.: Scaling of the velocity fluctuations in turbulent channels up to $\mathrm{Re}_\tau = 2{,}003$. Phys. Fluids **18**, 011702-1–011702-4 (2006)
19. Jaffrézic, B., Breuer, M., Chikhaoui, O., Deng, G., Visonneau, M.: Towards hybrid LES–RANS-coupling for complex flows with separation. In: Cancès, E., J.-F. Gerbeau (eds.) ESAIM: Proceedings, CEMRACS 2005, Computational Aeroacoustics and CFD in Turbulent Flows, Marseille, July 18–August 26, 2005, vol. 16, pp 89–113 (2007)
20. Jakirlić, S., Jester-Zürker, R., Tropea, C. (eds.) (2001) Report on 9th ERCOFTAC/IAHR/COST Workshop on Refined Flow Modeling. Darmstadt University of Technology, Germany, October 4–5, 2001
21. Keating, A., De Prisco, G., Piomelli, U., Balaras, E.: Interface conditions for hybrid RANS/LES calculations. In: Rodi, W. (ed.) Engineering Turbulence Modelling and Experiments, vol. 6, pp. 349–358 (2005)
22. Manceau, R., Bonnet, J.-P., Leschziner, M.A., Menter, F. (eds.): 10th Joint ERCOFTAC (SIG-15)/IAHR/QNET-CFD Workshop on Refined Flow Modeling. Université de Poitiers, France, Oct. 10–11, 2002
23. Mathey, F., Cokljat, D., Bertoglio, J.P., Sergent, E. (2003) Specification of LES inlet boundary condition using vortex method. In: Hanjalić, K., Nagano, Y., Tummers, M. (eds.) Turbulence, Heat and Mass Transfer IV. Begell House
24. Mellen, C.P, Fröhlich, J., Rodi, W.: Large-eddy simulation of the flow over periodic hills. In: Deville, M., Owens, R. (eds.) Proceedings of 16th IMACS World Congress, Lausanne, Switzerland (2000)
25. Ménéveau, C., Lund, T.S., Cabot, W.H.: A Lagrangian dynamic subgrid-scale model of turbulence. J. Fluid Mech. **319**, 353–385 (1996)
26. Moser, R.D., Kim, J., Mansour, N.N.: DNS of turbulent channel flow up to $Re_\tau = 590$. Phys. Fluids **11**, 943–945 (1999)
27. Nikitin, N.V., Nicoud, F., Wasistho, B., Squires, K.D., Spalart, P.R.: An approach to wall modeling in large-eddy simulations. Phys. Fluids **12**(7), 1629–1632 (2000)
28. Peller, N., Manhart, M.: DNS of the periodic hill flow test case at $Re_b = 5,600$. personal communication (2007)
29. Piomelli, U., Chasnov, J.R.: Large-eddy simulations: theory and applications. In: Hallbäck, M., Henningson, D.S., Johansson, A.V., Alfredson, P.H. (eds.) Turbulence and Transition Modelling, pp. 269–331, Kluwer, Dordrecht (1996)
30. Piomelli, U., Balaras, E., Pasinato, H., Squires, K.D., Spalart, P.R.: The inner-outer interface in large-eddy simulations with wall-layer model. Int. J. Heat Fluid Flow **24**, 538–550 (2003)
31. Pope, S.B.: Turbulent Flows. Cambridge University Press, Cambridge (2000)
32. Rhie, C.M., Chow, W.L.: Numerical study of the turbulent flow past an airfoil with trailing-edge separation. AIAA J. **21**, 1525–1532 (1983)
33. Rodi, W., Mansour, N.N., Michelassi, V.: One-equation near-wall turbulence modeling with the aid of direct simulation data. J. Fluids Eng. **115**, 196–205 (1993)
34. Sagaut, P.: Large eddy Simulation for Incompressible Flows—an Introduction. Springer, Heidelberg (2001)
35. Šarić, S., Jakirlić, S., Breuer, M., Jaffrézic, B., Deng, G., Chikhaoui, O., Fröhlich, J., von Terzi, D., Manhart, M., Peller, N.: Evaluation of detached-eddy simulations for predicting the flow over periodic hills. In: Cancès, E., J.-F. Gerbeau (eds.) ESAIM: Proceedings, CEMRACS 2005, "Computational Aeroacoustics and CFD in Turbulent Flows", Marseille, July 18–August 26, 2005, vol. 16, pp 133–145 (2007)
36. Schlüter, J.U., Pitsch, H., Moin, P.: Large-eddy simulation inflow conditions for coupling with Reynolds-averaged flow solvers. AIAA J. **42**(3), 478–484 (2004)
37. Schumann, U.: Subgrid-scale model for finite-difference simulations of turbulent flows in plane channels and annuli. J. Comput. Phys. **18**, 376–404 (1975)
38. Sergent, E.: Vers une Méthodologie de Couplage entre la Simulation des Grandes Echelles et les Modeles Stochastiques. Phd Thesis, Ecole Centrale de Lyon (2002)
39. Shur, M., Spalart, P.R., Strelets, M., Travin, A.: Detached-eddy simulation of an airfoil at high angle of attack. In: Rodi, W., Laurence, D. (eds) Fourth International Symposium on Engineering Turbulence Modeling and Measurements, Corsica, 24–26 May 1999. Engineering Turbulence Modeling and Experiments, vol. 4, Elsevier, Amsterdam, 1999, pp. 669–678 (1999)
40. Smagorinsky, J.: General circulation experiments with the primitive equations, I, The basic experiment. Month. Weather Rev. **91**, 99–165 (1963)
41. Spalart, P.R., Allmaras, S.R.: A one-equation turbulence model for aerodynamic flows. La Recherche Aérospatiale **1**, 5–21 (1994)
42. Spalart, P.R., Jou, W.-H., Strelets, M., Allmaras, S.R.: Comments on the feasibility of LES for wings, and on a hybrid RANS/LES approach. In: Liu, C., Liu, Z. (eds.) Advances in DNS/LES, 1st AFOSR International Conference on DNS/LES, August 4–8, 1997, Greyden, Columbus (1997)
43. Spalart, P.R.: Trends in turbulence treatments. AIAA Paper 2000–2306. In: FLUIDS 2000, Computational Fluid Dynamics Symposium, Denver, Colorado, USA, 19–22 June 2000
44. Spalart, P.R.: Strategies for turbulence modeling and simulations. Int. J. Heat Fluid Flow **21**, 252–263 (2000)
45. Speziale, C.G.: Turbulence modeling for time-dependent RANS and VLES: a review. AIAA J. **36**(2), 173–184 (1996)
46. Speziale, C.G.: A combined large-eddy simulation and time-dependent RANS capability for high-speed compressible flows. J. Sci. Comput. **13**, 253–274 (1998)
47. Strelets, M.: Detached-eddy simulation of massively separated flows. AIAA Paper 2001–0879 (2000)
48. Squires, K.D., Forsythe J.R., Spalart, P.R.: Detached-eddy simulation of the separated flow around a forebody cross-section. In: Geurts, B.J., Friedrich, R., Métais, O. (eds) Fourth Workshop on Direct and Large-eddy Simulation, Enschede, The Netherlands, 18–20 July 2001, ERCOFTAC Series, Direct and Large-eddy Simulation IV, Kluwer, Dordrecht, 2001, pp. 484–500 (2001)

49. Temmerman, L., Leschziner, M.A., Mellen, C.P., Fröhlich, J.: Investigation of wall-function approximations and subgrid-scale models in large eddy simulation of separated flow in a channel with streamwise periodic constrictions. Int. J. Heat Fluid Flow **24**, 157–180 (2003)
50. Temmerman, L., Hadžiabdić, M., Leschziner, M.A., Hanjalić, K.: A hybrid two-layer URANS-LES approach for large-eddy simulation at high Reynolds numbers. Int. J. Heat Fluid Flow **26**, 173–190 (2005)
51. Templeton, J.A., Medic, G., Kalitzin, G.: An eddy-viscosity based near-wall treatment for coarse grid large-eddy simulation. Phys. Fluids **17**, 105101-1–105101-6 (2005)
52. Travin, A., Shur, M., Strelets, M., Spalart, P.R.: Detached-eddy simulations past a circular cylinder. J. Flow Turbul. Combust. **63**(1/4), 293–313, Kluwer, Dordrecht (2000)
53. Travin, A., Shur, M., Strelets, M., Spalart, P.R.: Physical and numerical upgrades in the detached-eddy simulation of complex turbulence flows. In: Fluid mechanics and its application: advances in LES of complex flows (2002)
54. von Terzi, D., Hinterberger, C., García-Villalba, M., Fröhlich, J., Rodi, W., Mary, I.: LES with downstream RANS for flow over periodic hills and a model combustor flow. EUROMECH Colloquium 469, Large-eddy Simulation of Complex Flows, TU Dresden, Germany, October 6–8, 2005
55. Wagner, C., Hüttl, T., Sagaut, P. (eds.): Large-eddy Simulation for Acoustics. ISBN-13: 978052-187-1440, ISBN-10: 052-187-1441, Cambridge University Press, Cambridge (2007)
56. Wolfshtein, M.: The velocity and temperature distribution in one dimensional flow with turbulence augmentation and pressure gradient. Int. J. Heat Mass Transf. **12**, 301–318 (1969)
57. Yoshizawa, A., Horiuti, K.: A statistically-derived subgrid-scale kinetic energy model for the large-eddy simulation of turbulent flows. J. Phys. Soc. Jpn. **54**(8), 2834–2839 (1985)